Silencing ABAP1 INTERACTING PROTEIN 10 (AIP10) enhances root colonization by beneficial bacteria and improves plant performance under nutrient-limited conditions in *Arabidopsis thaliana*

Authors

Maria Clara Urquiaga[1±], Helkin Giovani Forero Ballesteros[1,2±], João Victor Silva[1], Patrícia Montessoro[1,2], Sara Gawantka Evangelista[1], Adriana Silva Hemerly[1*]

Affiliations

1- Laboratório de Biologia Molecular de Plantas, Instituto de Bioquímica Médica Leopoldo de Meis, Universidade Federal do Rio de Janeiro, Rio de Janeiro, RJ, Brazil
2- Hapiseeds Pesquisa e Desenvolvimento LTDA, Rio de Janeiro, RJ, Brazil (Present address)

± These authors have contributed equally to this work and share first authorship.
* Author for correspondence: hemerly@bioqmed.ufrj.br

1. Maria Clara Urquiaga: mariaclara.urquiaga@gmail.com (ORCID: 0000-0001-9539-6543)
2. Helkin Giovani F. Ballesteros: helfos85@gmail.com (ORCID: 0000-0001-5365-1841)
3. João Victor Silva de Oliveira: jvsilvaolivera.2001@gmail.com (ORCID: 0009-0000-4657-0242)
4. Patrícia Montessoro: patriciamontessoro@gmail.com (ORCID:0000-0001-7541-7714)
5. Sara Gawantka Evangelista: saragawantka@gmail.com (ORCID:0009-0008-9133-5856)
6. Adriana S. Hemerly: hemerly@bioqmed.ufrj.br (ORCID: 0000-0003-3748-7118)

Highlight

AIP10 silencing participates in a regulatory hub coordinating plant cell cycle and metabolism with recruitment of beneficial bacteria in the root microbiota, contributing to improved plant growth and productivity under nutrient-limited conditions.

Abstract

Sustaining high agricultural productivity with minimal environmental impact requires innovative and sustainable strategies that reduce reliance on mineral fertilizers. Promoting root association with plant growth-promoting bacteria (PGPB), either within the native microbiome or through bioinoculant application, represents a promising strategy to improve crop performance while reducing mineral fertilizer inputs. The success of this strategy, however, is strongly influenced by plant genetic traits that regulate microbial recruitment and colonization. Here, we tested whether silencing the ABAP1 Interacting Protein (AIP10), a negative regulator that links cell division with primary metabolism, modulates the association of *Arabidopsis thaliana* to PGPB. Non-inoculated *aip10-1* roots exhibited gene expression patterns similar to genotypes with enhanced microbial associations. *AIP10* silencing reshaped root and rhizosphere bacterial communities, favoring beneficial PGPB associations and limiting potential pathogens. Consistently, *aip10-1* plants showed greater colonization by inoculated diazotrophic PGPB, particularly in low fertilization conditions, leading to increased plant performance. These effects were accompanied by modulation of plant cell cycle and nitrogen assimilation pathways, together with increased bacterial colonization and *nifH* expression. Our findings suggest that AIP10 functions as a regulatory hub coordinating growth and metabolism with beneficial PGPB recruitment. Modulating AIP10 could enhance plant productivity and support more sustainable and regenerative agriculture practices.

Keywords: cell cycle, beneficial bacteria association, biological nitrogen fixation, microbiome, nutrient availability, ABAP1

1. Introduction

Global population growth has increased the demand for agricultural products, including food, bioenergy, and other bioproducts, while climate change negatively impacts agricultural productivity. To sustain high yields while protecting the environment, modern agriculture must develop innovative and sustainable technologies that reduce environmental impacts, particularly those associated with the excessive use of chemical fertilizers, which contribute to increased greenhouse gas (GHG) emissions ((Tilman *et al.*, 2011). In parallel, nitrogen use efficiency (NUE) is estimated to remain below 50% for many crop species ((Mueller *et al.*, 2019; Govindasamy *et al.*, 2023). Bioinoculants based on non-nodulating Plant Growth Promoting Bacteria (PGPB) represent a sustainable alternative to mineral fertilization, as they increase nutrients availability, improving soil fertility mainly through biological nitrogen fixation (BNF), mineral solubilization and iron-chelating siderophores production (Carvalho *et al.*, 2016; Omara *et al.*, 2019; Zuluaga *et al.*, 2020; Favero *et al.*, 2021; Pereira *et al.*, 2021; Rodrigues *et al.*, 2022) Furthermore, PGPB can stimulate plant development by synthesizing phytohormones, modulating antioxidant production, and altering the expression of defense-related genes, thereby enhancing plant tolerance to both biotic and abiotic stresses (Vargas *et al.*, 2014; Fukami *et al.*, 2017; Filgueiras *et al.*, 2020; Moretti *et al.*, 2021; Nunes *et al.*, 2021; Orozco-Mosqueda *et al.*, 2023).

Agriculturally important non-nodulating monocot crops, such as maize, rice and sugarcane, have shown beneficial responses to inoculation with bioinoculants based on non-nodulating diazotrophic bacteria (Hardoim *et al.*, 2020; Pankievicz *et al.*, 2021; Carvalho *et al.*, 2022; Ferrarezi *et al.*, 2022; Tian *et al.*, 2022). Although BNF in these crops is less efficient than in legumes, numerous studies have demonstrated that bacterial inoculation significantly increases grain yield and biomass with BNF contributing up to 37% of the total N in maize (Alves *et al.*, 2014; Di Salvo *et al.*, 2018; dos Santos *et al.*, 2020; Aquino *et al.*, 2021; Dias *et al.*, 2021). The use of PGPB bioinoculants represents a promising strategy for developing more resilient and productive crops. However, their efficient application still faces major challenges. The success of these interactions depends on both biotic and abiotic environmental factors, as well as on the host plant genotype by modulation of plant gene expression (Carvalho *et al.*, 2011, 2014; Vargas *et al.*, 2012). This modulation allows the host plant to recognize the bacterial strain as a beneficial partner and, in turn, regulate plant gene expression to facilitate PGPB colonization, thereby directly or indirectly activating plant pathways that promote plant growth (Carvalho *et al.*, 2011; Do Amaral *et al.*, 2014; Espindula *et al.*, 2019; Hardoim *et al.*,

111 2020; Ballesteros *et al.*, 2021; Pankievicz *et al.*, 2021; Thiebaut *et al.*, 2022; Rosman *et al.*,
112 2024).

113 Alterations in plant genes were shown to influence the assembly of root-associated
114 bacterial communities, indicating that root microbiome composition is strongly shaped by plant
115 genotype (Zang *et al.,* 2023). Modulation of defense-related pathways, such as salicylic acid
116 signaling, has been reported to affect the recruitment of specific bacterial groups in the
117 rhizosphere (Lebeis *et al.*, 2015). Likewise, genes involved in key signaling modules including
118 the PHR1–RALF–FERONIA pathway have been implicated in shaping root-associated
119 microbial communities with distinct functional capacities (Tang *et al.*, 2022). Additionally,
120 genes regulating the production of root-derived metabolites contribute to differences in
121 microbial composition and the enrichment of plant growth–promoting taxa (Stringlis *et al.*,
122 2018). These studies highlight that genetic variation in plants, including reductions in gene
123 activity, can play a significant role in determining the structure and function of the root
124 microbiome.

125 Plant plasticity, which allows the modulation of plant growth in response to different
126 environmental cues, including association with PGPB that enhance plant biomass and
127 productivity. Ultimately, biomass increases are driven by higher rates the regulation of cell
128 division rates (Qi and Zhang, 2020; Pierik *et al.*, 2021; Zluhan-Martínez *et al.*, 2021). Recently,
129 our group described a novel cell cycle regulator, the ABAP1 Interacting Protein 10 (AIP10),
130 which acts in a central hub integrating cell division rates with transcriptional reprogramming
131 of basal metabolism (Montessoro *et al.*, 2025). This role is mediated by AIP10 protein
132 interactions with the Armadillo BTB Arabidopsis protein 1 (ABAP1), a negative regulator of
133 the cell cycle in plants, with KIN10, a catalytic subunit of the Sucrose non-fermenting-1-related
134 protein kinase 1 (SnRK1), and possibly additional partners (Masuda *et al.*, 2008; Montessoro
135 *et al.*, 2025). In *Arabidopsis thaliana, aip10-1* knockout mutant plants exhibited increased cell
136 division rates, resulting in enhanced shoot and root vegetative growth, as well as higher
137 numbers of silique and seed production (Montessoro *et al.*, 2025). In addition, reduced *AIP10*
138 expression triggered a major transcriptional reprogramming of plant primary metabolism
139 mediated by SnRK1, leading to increased photosynthetic and water use efficiency and greater
140 carbon fixation that met plant energy demands for increased biomass accumulation, and higher
141 contents of proteins, lipids and carbohydrates (Montessoro *et al.*, 2025).

142 Developing strategies that enhance plant-bacteria interaction is a promising approach
143 to increasing agricultural productivity and promoting more sustainable agriculture. *A. thaliana*
144 was already used as a model system to assess developmental responses and proteomic changes

145 triggered by association with PGPB, such as endophytic diazotrophic bacteria (Cohen *et al.*,
146 2015; Souza *et al.*, 2016; Leandro *et al.*, 2019; Dos Santos *et al.*, 2020). Here, we evaluated the
147 role of AIP10 in interactions with PGPB, both within the native root microbiota and following
148 inoculation with PGPB-based inoculants. The previously described *aip10-1* full knockout
149 mutant was used as a functional model and investigated using multiple complementary
150 approaches, including RT-qPCR and RNA-seq gene expression profiling, root and soil
151 microbiome metabarcoding, PGPB inoculation and comprehensive plant phenotyping. The
152 transcriptional profile of non-inoculated *aip10-1* roots resembled signatures of genotypes with
153 enhanced capacity to interact with beneficial microorganisms. Loss of *AIP10* function reshaped
154 root-associated bacterial communities, in roots and rhizospheric soil, favoring the recruitment
155 of beneficial PGPB species while reducing potentially pathogenic taxa. Accordingly, *aip10-1*
156 plants showed higher colonization by inoculated diazotrophic PGPB, leading to improved
157 vegetative and reproductive growth. Moreover, under low fertilizer conditions, *aip10-1* plants
158 exhibited a stronger response to PGPB bioinoculants, achieving biomass levels similar to non-
159 inoculated plants grown under high fertilization. These findings indicate that AIP10 silencing
160 is a promising strategy to enhance PGPB colonization and improve nutrient use efficiency
161 under reduced chemical fertilization, contributing to a more sustainable and regenerative
162 agriculture.
163

164 ## 2. Material and Methods

165 ### *2.1. Bacterial strains and growth conditions*

166 For plant inoculation, the diazotrophic bacterial strain *Gluconacetobacter*
167 *diazotrophicus* PAL5 DsRed, labeled with red fluorescent protein and *Herbaspirillum*
168 *seropedicae* RAM10, labeled with green fluorescent protein, kindly provided by Dr. Gonçalo
169 Apolinário de Souza Filho (State University of Norte Fluminense Darcy Ribeiro), and
170 *Herbaspirillum seropedicae* HRC54 (BR11335), obtained from EMBRAPA Agrobiologia
171 (Rio de Janeiro, Brazil), were used. Additionally, the commercial biofertilizer BioFree® (liquid
172 formulation), supplied by BioFROST and registered with the Brazilian Ministry of Agriculture,
173 Livestock and Food Supply (MAPA, No. PR001593-8.000001), containing *Azospirillum*
174 *brasilense* Ab-V6 and *Pseudomonas fluorescens* CCTB03 (1×10^{11} CFU/L), was employed in
175 the assays. *G. diazotrophicus* PAL5 DsRed was cultured in LGI-P medium (100 g/L granulated
176 sugar; 2 mL/L K_2HPO sol. 10%; 6mL/L KH_2PO_4 sol. 10%; 2 mL/L $MgSO_4.7H_2O$ sol. 10%; 2
177 mL/L $CaCl_2.2H_2O$ sol. 1%; 1 ml/L $FeCl_3.6H_2O$ sol. 1%; 2 mL/L $Na_2MoO_4.2H_2O$ sol. 0.1%; 5

178 mL/L bromothymol blue sol. 5% w/v in 0.2N KOH; pH 5.8) supplemented with streptomycin
179 (50 mg/L) and 1 mL of vitamin stock solution (biotin 100mg/L; pyridoxal-HCL 200 mg/L)
180 per liter of medium (Baldani *et al.*, 1996) and *H. seropedicae* HRC54 was grown in JNFB
181 medium (5 g/L malic acid; 6 mL/L K_2HPO sol. 10%; 18 mL/L KH_2PO_4 sol. 10%; 2 mL/L
182 $MgSO_4.7H_2O$ sol. 10%; 1 mL/L NaCl sol. 10%; 2 mL/L bromothymol blue sol. 5% w/v in
183 0.2N KOH; 4 mL/L FeEDTA sol. 1.64%; 4 g/L KOH; 1,07 g/L NH_4Cl; pH 6.0) supplemented
184 with 1 mL of vitamin stock solution and 2 mL of micronutrients stock solution (1 g/L
185 $Na_2MoO_4.2H_2O$; 1.175 g/L MnSO.HO; 1.4 g/L HBO; 0.04 g/L CuSO.5HO; 0.12 g/L
186 ZnSO.7HO) per liter (Baldani *et al.*, 1996). Both strains were subsequently transferred to
187 DYGS liquid medium (2 g/L malic acid; 2 g/L glucose; 1.5 g/L bacteriological peptone; 2 g/L
188 yeast extract; 0.5 g/L K_2HPO_4; 0.5 g/L $MgSO_4.7H_2O$ and 1.5 g/L glutamic acid, pH 6.0 for
189 HRC54 and pH 5.8 for Pal5 without malic acid) (Baldani *et al.*, 1996) and incubated at 30 °C
190 with agitation (200 rpm) for 6–12 hours until reaching an optical density at 660 nm of
191 approximately 0.8, corresponding to ~10^8 cells mL^{-1}. For plant inoculation, bacterial cultures
192 and the commercial inoculant were diluted 1:1000 (v/v) in autoclaved distilled water.

193 ***2.2. Plant material and inoculation with plant-growth promoting bacteria***

194 Seeds of the wild-type *A. thaliana* ecotype Col-0 and the knockout mutant line *aip10-*
195 *1* (SALK_022332, T-DNA insertion), obtained from the Salk collection (Salk Institute
196 Genomic Analysis Laboratory) and previously characterized (Montessoro *et al.*, 2025), were
197 used for the AIP10 functional analyses. The seeds were sterilized by exposure to chlorine gas,
198 generated by the reaction between 97 mL of bleach (4.3%) and 3 mL of hydrochloric acid
199 (37%). After 2 hrs of treatment, the seeds were left in a laminar flow hood until the gas had
200 completely evaporated. Then, they were sown in Petri dishes containing Murashige and Skoog
201 (MS) ½ medium, supplemented with 0.05% 2-(N-morpholino) ethanesulfonic acid (MES), 1%
202 sucrose and 0.8% Phytagel (Sigma-Aldrich®), adjusted to pH 5.7. Seeds were stratified at 4
203 °C for 2 days and subsequently grown vertically in a growth chamber with a 12/12 hrs
204 photoperiod at 21 °C.

205 Four days after germination (4 DAG), 2 µL of the diluted bacterial suspension (1:1000),
206 containing approximately 10^2 cells μL^{-1}, were applied to the root zone. Control seedlings were
207 mock-treated with sterile DYGS medium diluted in the same proportion. After inoculation, the
208 seedlings were transferred to Petri dishes containing modified MS ½ medium (sucrose-free)
209 and maintained under the same culture conditions for another 7 days, totaling 11 DAG. For
210 molecular analyses, three biological replicates per treatment were harvested at 11 DAG, with

211 shoots and roots separated, frozen in liquid nitrogen, and stored at −80 °C. Plants were then
212 transplanted into pots containing a standard mixture of substate:vermiculite (3:1, w/w) and
213 grown under a 16/8 hrs photoperiod at 21 °C until 17 DAG.

214 In the experiment with different nutritional doses, after a 6-day acclimatization period,
215 the plants were watered with two different concentrations of NPK 20-20-20 fertilizer, defined
216 as low nutrient availability (final concentration of 0.06 g/L, corresponding to 12 mg/L N, 5.2
217 mg/L P and 10 mg/L K) and high nutrient availability (final concentration of 0.12 g/L,
218 corresponding to 24 mg/L N, 10.4 mg/L P and 20 mg/L K).The plants were harvested 31 days
219 after inoculation (31 DAI), corresponding to 35 DAG, for phenotypic analysis, and their
220 productivity was evaluated at 60 DAG.

221 ***2.3. Phenotypic analyses of A. thaliana plants***

222 Phenotypic analyses were performed on *A. thaliana* plants after separating shoots and
223 roots at 31 DAI. Fresh matter weight was measured using an analytical precision balance with
224 eight biological replicates. Thereafter, shoot and root samples were then placed in paper bags
225 and oven-dried at 60 °C for 6 days. Dry weight was subsequently measured using the same
226 balance, with eight biological replicates, to determine biomass. In addition, the rosette area was
227 determined from images evaluated in imageJ software (Schindelin *et al.*, 2012). The values of
228 fresh and dry matter and rosette area obtained were statistically analyzed using GraphPad Prism
229 software version 8.0.0. Statistical analysis was performed using Student's T-test. Statistical
230 significance was defined in all cases as p-value < 0.05

231 To analyze root development, harvested roots were immersed in 70% ethanol for 7
232 days. Subsequently, roots were laid out in an acrylic container (10 × 45 cm), with water at an
233 approximate depth of 1 cm for scanning. They were then characterized by image analysis using
234 WinRHIZO Pro® software (Regent Instruments, QC, Quebec, Canada) coupled to an Epson
235 Expression 11000XL LA2400 image scanner, as described in previous works (Bauhus and
236 Messier, 1999). Root length (cm) and surface area (m^2) were evaluated in five plants per
237 treatment. All analyzes used the Student's T-test. Statistical significance was defined as p-value
238 < 0.05.

239 Productivity analyses were performed at 56 DAI (60 DAG), including measurements
240 of number of siliques, length of the main inflorescence axis, and weight of seeds per plant. The
241 resulting data were subjected to statistical analysis using GraphPad Prism software version
242 8.0.0. Statistical significance was assessed using Student's T-test. The significance level of p
243 < 0.05 was used to determine statistical significance across all analyses.

244

245 ***2.4. Photosynthetic pigments***

246 Chlorophyll *a* and chlorophyll *b* were extracted at 31 DAI using dimethyl sulfoxide
247 (DMSO). Two rosette discs from the fifth leaf were incubated in 1 mL of DMSO for 72 h at
248 room temperature in the dark. Absorbance was measured at 480, 649.1, and 665.1 nm
249 (NanoDrop™ 2000), and pigment concentrations were calculated based on standard equations
250 ($Ca = 12.74 \times A665.1 - 3.62 \times A649.1$; $Cb = 25.06 \times A649.1 - 6.5 \times A665.1$). Results were
251 expressed as µg/g fresh weight. Statistical analysis was based on the Student's T-test for all
252 comparisons. Statistical significance was defined as p-value < 0.05.

253 ***2.5. RNA extraction and Real-time quantitative PCR***

254 For molecular analyses, plant roots were macerated in liquid nitrogen and immediately
255 stored at −80°C. At 11 DAG, total RNA was extracted from inoculated and non-inoculated
256 samples of each genotype using a lithium chloride–based protocol, as described by (Logemann
257 *et al.*, 1987). RNA concentration was determined with a NanoDrop™ 2000c spectrophotometer
258 (Thermo Scientific, USA), and its integrity was assessed by electrophoresis in a 1% agarose
259 gel stained with ethidium bromide. Approximately 5 µg of total RNA was treated with DNase
260 I (Biolabs), according to the manufacturer's instructions, and used for the synthesis of the first
261 strand of cDNA with GoScript reverse transcriptase (Promega). Gene expression analyses were
262 performed by RT-qPCR using SYBR Green PCR Master Mix (Applied Biosystems). Each
263 reaction was assembled in a final volume of 10 µL, containing 2 µL of cDNA diluted 1:3, 5 µL
264 of SYBR Green mix, 1 µL of each primer (forward and reverse, 10 µM) and 1 µL of sterile
265 ultrapure water. The primers specific for the target genes analyzed are listed in Table S1.
266 Expression normalization was performed based on the constitutive genes *UBIQUITIN 14*
267 (*UBI14*) and *GLYCERALDEHYDE-3-PHOSPHATE DEHYDROGENASE* (*GAPDH*) of *A.*
268 *thaliana*. Data analysis followed the ΔCT method, based on the subtraction of the CT value of
269 the constitutive gene in relation to the target gene. All experiments were conducted with three
270 biological replicates per condition.

271 ***2.6. DNA extraction and Real time quantitative PCR absolute bacterial quantification***

272 Total DNA extraction was performed using CTAB 2% protocol (Doyle and Doyle,
273 1987). DNA concentration was determined with a NanoDrop™ 2000c spectrophotometer, and
274 its integrity was assessed by electrophoresis in a 1% agarose gel stained with ethidium bromide.
275 Total DNA was treated with 0,01g/mL RNase A and incubated at 37 ºC for 1 h. To determine

276 the bacterial cell number cells (cells g^{-1} plant tissue), the average Ct value from two technical
277 replicates for each DNA sample was used to quantify *G. diazotrophicus* PAL5, *H. seropedicae*
278 HRC54, *A. brasilense* Ab-V6. Genus-specific standard curve equations, previously established
279 in the laboratory, were applied for quantification. The number of cells were inferred from the
280 amplicon copy number, assuming the target sequence is single copy per genome. Target-
281 specific primer pairs are listed in Table S1. For each treatment, cells per gram of tissue were
282 calculated from the DNA samples using the following equation: Absolute number of cells = A
283 × B (ng μL^{-1}) × C (μL) / D (ng) × E (g). Where, A = number of fragment copies, obtained from
284 the strain-specific standard curve; B = Concentration of extracted genomic DNA; C = volume
285 of DNA extracted; D = amount of DNA used in the qPCR reaction; E = initial plant tissue mass
286 used for DNA extraction.

287 ***2.7. Metagenomic Barcode Analysis***

288 Plants used in the metagenomic barcode analysis experiment were grown under the low
289 nutrient condition protocol and collected at 20 DAG. For each genotype Col-0 wild type and
290 *aip10-1* plants, one sample pool consisting of three plants was collected. Metagenomic barcode
291 analysis experiment was performed exclusively from the root tissue of each genotype. Soil
292 samples were obtained as a sample pool composed of material from the three pots
293 corresponding to the plants whose roots were collected.

294 Total DNA was extracted separately from root and rhizosphere soil samples of *A.*
295 *thaliana* Col-0 and the mutant *aip10-1* using a commercial soil DNA extraction kit. The V3–
296 V4 regions of the bacterial 16S rRNA gene were amplified with universal primers containing
297 Illumina adapters, and amplicon libraries were prepared following standard protocols.
298 Sequencing was performed on an Illumina MiSeq platform (PE 500 bp). Taxonomic
299 assignment was performed against the SILVA 138 database, with removal of non-bacterial
300 sequences. Relative abundance of bacterial taxa was calculated separately for root and soil
301 samples, and results were visualized using GraphPad Prism 10.5.0 for bar plots and
302 comparisons between genotypes. Heatmaps of selected PGPB, diazotrophs, and pathogens
303 were generated in R (pheatmap package), based on log-transformed relative abundances and
304 hierarchical clustering.

305 ***2.8. Confocal microscope and microscopic analysis***

306 Roots of *A. thaliana* ecotype Col-0 wild type and *aip10-1* inoculated with *G. diazotrophicus*
307 Pal5-RFP and *H. seropedicae* RAM10-GFP were analyzed 7 DAI. Imaging was conducted

308 using a Leica TCS SPE confocal microscope. Plant samples were mounted on microscope
309 slides with a drop of water and covered with a coverslip for observation under a light
310 microscope. For RFP observation (from *G. diazotrophicus* Pal5-RFP), samples were excited at
311 568 nm and emission was collected at 640 nm. For *H. seropedicae* RAM10-GFP (BR 11335),
312 samples were excited at 475 nm and emission was collected at 509 nm. Differential interference
313 contrast (DIC) images were also captured simultaneously using bright field. Image acquisition
314 and processing were performed using Leica LAS AF software.
315

316 ## 3. Results

317 ***AIP10 expression profile in response to plant growth-promoting bacteria***

318 To explore the relationship between PGPB association, plant genotype, and *AIP10*
319 expression, we examined the transcriptional profile of the sugarcane (*Saccharum spp.*) *AIP10*
320 homologue based on previously published RNA-seq datasets from two genotypes differing in
321 their capacity to associate with beneficial bacteria and to sustain BNF: SP70-1143 (high BNF)
322 and Chunee (low BNF) (Urquiaga and Boddey, 1992; Carvalho *et al.*, 2022). Transcript levels
323 were analyzed in root and shoot tissues from plants grown under natural bacterial colonization
324 and bacteria-free hydroponic conditions. Fold change values (SP70-1143/Chunee) were
325 calculated based on RPKM values to compare the genotype with higher association efficiency
326 with diazotrophic bacteria to the less efficient genotype.

327 Under natural colonization conditions, the *AIP10* homolog exhibited lower expression
328 levels in both roots and shoots of the high-BNF genotype SP70-1143 relative to Chunee (Fig.
329 1A). In contrast, under bacteria-free conditions (BF), *AIP10* expression was upregulated in
330 both tissues root and shoot of SP70-1143. These results indicate that *AIP10* expression is
331 reduced in the genotype exhibiting higher BNF capacity when associated with beneficial
332 bacteria, supporting its role as a negative regulator of plant growth, and suggesting its
333 modulation may participate in growth promotion in response to beneficial plant-bacteria
334 interaction.

335 A comparative protein domain analysis revealed that AIP10 proteins from *A. thaliana*
336 and sugarcane share a conserved domain architecture, including predicted nuclear localization
337 signals (NLS) and coiled-coil domains (Fig. 1B). This high level of structural conservation
338 suggests a conserved regulatory function of AIP10 across monocot and dicot species. In
339 agreement with these findings, the data revealed a similar *AIP10* expression profile in both
340 plant species, suggesting that these proteins may share similar biological functions.

341 Comparative protein domain analysis of two AIP10 orthologous isoforms in *A. thaliana*
342 (AT1G80940.1 and AT1G80940.3) and one putative isoform in *S. spontaneum*
343 (Sspoon.04G0001710-3D) further confirmed the conservation of nuclear localization and
344 coiled-coil domains, while revealing the presence of an additional ribosomal L32e domain in
345 the sugarcane protein.

346 Next, we investigated the modulation of *AIP10* expression profile by inoculation with
347 beneficial PGPB in Col-0 plants from *A. thaliana*. Plant material was collected at 7 DAI with
348 the diazotrophic PGPB *H. seropedicae* or *G. diazotrophicus,* to assess the *AIP10* transcriptional
349 response during the early stages of plant–microbe interaction (Fig. 1C). The results showed a
350 significant repression of *AIP10* expression in response to both bacterial strains compared to
351 mock-treated controls, with a stronger down-regulation observed upon inoculation with *H.*
352 *seropedicae* (Fig. 1C). These data suggest that *AIP10* expression is reduced during early stages
353 of plant-PGPB interactions. Together, the results indicate that AIP10 displays a conserved
354 domain architecture across species, while its expression is differentially modulated by bacterial
355 colonization in sugarcane genotypes contrasting for BNF efficiency and in *A. thaliana*.

356 To explore molecular pathways involved in plant–microorganism interactions
357 potentially modulated by *AIP10* repression, we reanalyzed previously generated RNA-seq data
358 in the root transcriptomes of *A. thaliana* Col-0 and *aip10-1* at 11 DAG (Montessoro *et al*.,
359 2025). We examined enriched functional categories across metabolic pathways related to Cell
360 wall formation, Response to stimuli, Immune response to bacteria, Responses to hormones,
361 Responses to lipids, Carbohydrates and General metabolic Processes (Fig. S1).

362 In cell wall–related categories, genes directly involved in cell wall reinforcement and
363 stress-associated remodeling were downregulated (Fig. S1A), including *EXT15* (*Extensin 15*,
364 AT1G23720), *LRX3* (*Leucine-rich repeat extensin 3*, AT4G13340) and LRX4 (At3g24480.
365 The repression of extensins and LRX proteins, which are essential for cell wall assembly,
366 integrity, and mechanical strength, suggests increased cell wall plasticity that may facilitate
367 bacterial association and root tissue colonization (Draeger *et al.*, 2015; Kandel *et al.*, 2017). A
368 distinct group of proteins associated with cell wall expansion and extracellular matrix
369 organization was significantly induced at 11 DAG, including *GASA1* (Gibberellic Acid
370 Stimulated Arabidopsis 1, AT1G75750) and *LCR69* (Low-molecular-weight Cysteine-rich
371 protein 69, AT2G02100), suggesting enhanced wall loosening and elongation processes.
372 Consistent with this pattern of cell wall modification, genes encoding enzymes involved in
373 polysaccharide modification and pectin remodeling were also upregulated, including *PME46*
374 (Pectin Methylesterase 46, AT5G04960), *XHT* (Xyloglucan endotransglucosylase/hydrolase,

375 AT4G25820), and *ATTIP2* (Tonoplast Intrinsic Protein 2, AT3G16240). These changes
376 suggest active restructuring of the polysaccharide network that regulates wall extensibility and
377 porosity in *aip10-1* plants, potentially enhancing apoplastic permeability and promoting cell-
378 to-cell communication (Dora *et al.*, 2022).

379 In the hormone-responsive category, the auxin-responsive genes *SAUR69* (Small Auxin
380 Upregulated RNA 69) and *SAUR72* (Small Auxin Upregulated RNA 72) were strongly
381 upregulated, suggesting a role in promotion of plant growth. Up-regulation of *RSL4* (*bHLH85*,
382 ROOT HAIR DEFECTIVE 6-LIKE 4), a transcription factor, that positively regulates root hair
383 development, was upregulated in *aip10-1* roots. Enhanced root hair growth is a commonly
384 reported response to inoculation with PGPB (Zhao et al., 2025).

385 Some genes involved in defense or immunity pathways associated with bacterial
386 interactions were repressed, whereas others were upregulated in *aip10-1* roots, consistent with
387 the regulatory adjustments required for beneficial associations with PGPB (Carvalho et al,
388 2016; Stringlis *et al.*, 2018). Among the most downregulated genes were *CYP71A12* and
389 *CYP71A13* (Cytochrome P450 71A12 and– Cytochrome P450 71A13), which are key enzymes
390 involved in camalexin and tryptophan-derived secondary metabolite biosynthesis. Their
391 repression suggests a reduction in defense pathways. In contrast, a distinct subset of bacterium-
392 responsive genes was strongly induced, reflecting activation of regulatory pathways associated
393 with plant–microbe communication and systemic signaling. A subset of stimulus-related genes,
394 including *PDF2.2* (*Plant Defensin 2.2*), *ATL15* (*RING-type E3 ubiquitin ligase 15*),
395 AT1G22770, and AT1G15010, was induced, suggesting the activation of regulatory and
396 antimicrobial components that may contribute to controlling the number of bacteria that could
397 associate with and colonize the root tissue. The most strongly induced gene was *ILA*
398 (ILITHYIA), which is required for plant immunity and is directly associated with basal defense
399 in *A. thaliana* against the pathogenic bacteria *Pseudomonas syringae* (Monaghan and Li, 2010).
400 It also plays a central role in coordinating developmental and immune signaling (Faus *et al.*,
401 2018).

402 Regulation of metabolic, lipid, and carbohydrate-responsive genes in *aip10-1* revealed
403 coordinated transcriptional reprogramming affecting primary metabolism and stress-associated
404 pathways. Repression of *PAD3* (Phytoalexin Deficient 3) and *CBP60G* (Calmodulin-Binding
405 Protein 60G) supports an attenuation of defense-related metabolic pathways, indicating a
406 general downregulation of stress-associated programs. Within this metabolic shift, genes
407 involved in carbohydrate-related processes also showed regulatory adjustments. In particular,
408 repression of *GLS1* (Glucan Synthase-Like 1) together with induction of *ATL15* (RING-Type

409 E3 Ubiquitin Ligase 15) suggests a reprogramming of carbon-associated regulation, reflecting
410 an adjustment of carbohydrate metabolism rather than a simple reduction in carbon availability.
411 Together, the transcriptional changes observed in *AIP10*-silenced plants revealed
412 modulation of core metabolic processes coupled with regulation of defense and growth-related
413 pathways. These changes are consistent with transcriptional reprogramming associated with
414 plant responses to beneficial endophytic or associative PGPB and aligned with the effects of
415 reduced *AIP10* expression observed under natural bacterial colonization in sugarcane.
416
417 ***Root-associated microbiota composition in A. thaliana wild-type and aip10-1 plants***
418 Given that transcriptional reprogramming in *aip10-1* plants affected multiple pathways
419 related to plant–microbe interactions, we next examined whether AIP10 silencing altered the
420 composition of the root-associated microbiota in *A. thaliana*. A metagenomic barcode analysis
421 of the root-associated bacterial communities and the rhizosphere soil of non-inoculated Col-0
422 and *aip10-1* plants was performed.
423 The Venn diagram revealed a complex distribution of shared and unique taxa among
424 the four sample types, comprising soil and roots from both genotypes. Col-0 and *aip10-1* roots
425 each harbored a high number of genotype-specific bacterial species (237 and 203, respectively)
426 (Fig. 2A), indicating distinct recruitment patterns. Despite these differences, a substantial core
427 microbiome of 975 bacterial species was shared across all samples, highlighting a conserved
428 microbial baseline between soil and plant genotypes. Additionally, soil samples associated with
429 Col-0 and *aip10-1* each contained unique taxa (173 and 220 species, respectively) (Fig. 2A),
430 reflecting environmental and genotype-driven filtering effects. Together, these findings
431 demonstrate that *AIP10* silencing reshapes root-associated bacterial communities while
432 maintaining a large portion of shared microbial taxa.
433 For a more focused assessment of functionally relevant components of the native
434 microbiome potentially associated with growth promotion and innate immune responses in the
435 host plant, the abundance of selected bacterial categories was analyzed by z-score values (Table
436 S2), including potential diazotrophic bacteria, PGPB, and plant pathogenic bacteria.
437 Comparative profiling of bacterial communities associated with the plant root
438 compartment revealed pronounced differences between Col-0 and *aip10-1* genotypes (Fig. 2B-
439 C). At the species level, roots of *aip10-1* plants exhibited increased relative abundance of
440 several potential diazotrophic bacteria, including, *Azospirillum brasilense* (z-score 1,4),
441 *Azospirillum halopraferens* (z-score 1,5), *Bradyrhizobium elkanii* (z-score 1,4) and
442 *Bradyrhizobium guangxiense* (z-score 0,9). In addition, plant PGPB species were enriched in

443 *aip10-1* roots in comparison with Col-0 roots, as *Paenibacillus medicaginis* (z-score 0,9) (Fig.
444 2C).
445 In contrast, roots of Col-0 plants displayed higher relative abundance of several
446 pathogenic species, compared to *aip10-1* roots (Fig. 2D). Taxa such as *Xanthomonas*
447 *arboricola* (z-score 1,5), *Xanthomonas axonopodis* (z-score 0,5), *Pantoea brenneri* (z-score
448 1,5), and *Erwinia soli* (z-score 0,4) were comparatively more abundant in Col-0 and were not
449 detected in *aip10-1*. These data suggest that *aip10*-1 plants tend to preferentially recruit and
450 associate with specific beneficial PGPB species in the root compartment while being depleted
451 in potentially pathogenic taxa.
452 A similar pattern was observed in soil-associated bacterial communities (Fig. 2B-C).
453 Soils cultivated with *aip10-1* plants were characterized by increased relative abundance of
454 several potential diazotrophic species, including *Mesorhizobium composti* (z-score 31,2),
455 *Mesorhizobium gobiense* (z-score 52,7), *Mesorhizobium hankyongi* (z-score 1,0),
456 *Mesorhizobium silamurunense* (z-score 3,7) *Azospirillum formosense* (z-score 1,5),
457 *Burkholderia alpina* (z-score 6,3), *Burkholderia ultramafica* (z-score 0,7), when compared
458 with soils from Col-0 plants. Likewise, PGPB species such as *Paraburkholderia diazotrophica*
459 (z-score 1,1), *Paraburkholderia megapolitana* (z-score 1,2), *Paraburkholderia metrosideri* (z-
460 score 0,9) and *Bradyrhizobium canariense* (z-score 0,9) were more abundant in soils associated
461 with *aip10-1*.
462 On the other hand, soils from Col-0 plants harbored higher relative abundances of
463 potential pathogenic species (Fig. 2D), including *Xanthomonas campestris* (z-score 1,5),
464 *Xanthomonas translucens* (z-score 1,5), *Erwinia billingiae* (z-score 1,5), and *Agrobacterium*
465 *larrymoorei* (z-score 1,5). Together, these results suggest that the loss of AIP10 function
466 reshapes the root-associated bacteria in roots and rhizospheric soil, increasing the prevalence
467 of beneficial bacteria while reducing potential pathogens.
468
469 ***Efficiency of PGPB bioinoculant colonization in aip10-1 plants***
470 As *AIP10* silenced mutants showed increased abundance of beneficial bacteria in their
471 root microbiome, we next investigated whether *aip10-1* mutants exhibited enhanced
472 colonization in response to inoculation with diazotrophic PGPB bioinoculants, compared to
473 wild-type Col-0 plants, by quantifying and assessing the dynamics of bacterial root
474 colonization.
475 Initially, an *in vitro* inoculation system followed by greenhouse cultivation was
476 established to study the interaction of *aip10-1* mutant plants with two N_2-fixing bacterial

477 strains, *H. seropedicae* HRC54 or *G. diazotrophicus* Pal5. Representative images of *aip10-1*
478 plants at 20 DAG, inoculated with either strain, are shown in Fig. 3A. Under *in vitro* growth
479 conditions, root architectural parameters were evaluated revealing that inoculated *aip10-1*
480 plants displayed a significant increase in primary root length compared with mock-treated
481 plants and inoculated Col-0 controls (Fig. 3B). In addition, the number of lateral roots was
482 significantly higher in inoculated *aip10-1* plants, particularly in response to PAL5 (Fig. 3C).
483 To determine whether these early root architectural changes translate into later
484 developmental outcomes, shoot-related traits were assessed at later developmental stages. At
485 21 DAG, *aip10-1* plants inoculated with both bacterial strains accumulated significantly higher
486 shoot biomass (Fig. 3D) and developed larger rosette areas compared with Col-0 plants and
487 mock-treated controls (Fig. 3E).
488 Quantification of bacterial colonization based on absolute values of single-copy
489 bacterial gene using genus-specific primers showed that *aip10-1* roots of inoculated plants were
490 better colonized by both bioinoculants, compared to wild-type Col-0 roots (Fig. 3F and G). To
491 evaluate if the higher colonization by *G. diazotrophicus* or *H. seropedicae* was correlated with
492 actively metabolic bacteria, *nifH* mRNA expression was analyzed. The *nifH* is present in most
493 diazotrophic microorganisms and encodes a key component of nitrogenase, making it an ideal
494 marker for assessing the stimulation of N_2-fixation metabolism in bacterial communities
495 (Nichio *et al.*, 2025). As shown in Fig. 3H and I, PGPB-inoculated *aip10-1* plants showed
496 significantly higher relative expression of *nifH* than inoculated wild-type plants during
497 association with both HRC54 or PAL5, respectively.
498 To investigate whether *aip10-1* mutants affect the niche of bacterial colonization in root
499 tissues, RFP- and GFP-labeled G. *diazotrophicus* and *H. seropedicae* bacteria, respectively,
500 were used as bioinoculants and monitored by confocal microscopy. The data showed
501 differences in Col-0 and *aip10-1* roots in relation to the pattern of bacterial colonization. In
502 mock Col-0 roots, both RFP- and GFP-labeled bacteria showed minimal and discontinuous
503 fluorescence, indicating low colonization levels. In contrast, inoculated *aip10-1* roots displayed
504 strong and spatially extended fluorescent signals, with well-defined aggregates and continuous
505 bands along the root surface (Fig. 3J). A detailed analysis of distinct root regions further
506 demonstrated that these differences were spatially structured. In the meristematic zone, both
507 genotypes exhibited low colonization (Fig. S2). However, beginning in the root hair zone,
508 *aip10-1* showed a marked increase in bacterial attachment, with continuous fluorescent bands
509 extending along the root axis. This pattern became more evident in the elongation zone, where
510 large portions of the cortex and epidermis were covered by bacteria, in sharp contrast to the

511 fragmented and sparse pattern observed in Col-0 (Fig. S2). The highest colonization levels
512 were observed at lateral root emergence sites, where inoculated aip*10-1* roots displayed
513 extensive and well-defined bacterial aggregates, whereas Col-0 presented only small, scattered
514 foci. Together, these spatial colonization patterns indicate that loss of AIP10 enhances root
515 colonization, particularly in regions of active growth and lateral root formation, resulting in
516 greater density, continuity, and stability of bacterial association.
517 Together, these results indicate that *AIP10* silencing is associated with enhanced
518 bacterial colonization and activity in roots, accompanied by pronounced changes in root
519 architecture and shoot growth following inoculation.
520
521 ***Molecular mechanisms of plant growth promotion in PGPB inoculated aip10-1 plants***
522 As *AIP10* silenced mutants showed increased root colonization by beneficial bacteria
523 and enhanced plant growth promotion, compared to wild-type Col-0 plants, we investigated
524 the molecular mechanisms that may contribute to the improved responsiveness of *aip10-1*
525 plants to PGPB bioinoculants.
526 First, we investigated the modulation of cell division controls in inoculated *aip10-1* and
527 Col-0 plants. AIP10 has previously been described as a negative modulator of cell division,
528 through its interaction with ABAP1 and regulation of ABAP1 target gene expression
529 (Montessoro *et al.*, 2025). Also, *ABAP1* expression is negatively regulated in *aip10-1* mutants.
530 Therefore, the expression levels of *ABAP1* and *CDT1a*, a target gene negatively regulated by
531 ABAP1 and a positive marker of DNA replication, were evaluated by RT-qPCR (Fig. 4). In
532 *aip10-1* plants, *ABAP1* expression was more strongly repressed following inoculation with
533 PAL5 and HRC54 compared to mock-treated mutants, whereas inoculated Col-0 plants
534 consistently exhibited higher *ABAP1* expression than *aip10-1* mutants (Fig. 4A). Accordingly,
535 *CDT1a* expression was induced in *aip10-1* plants in response to both beneficial inoculations,
536 with PAL5 triggering significantly higher induction than in mock-treated plants (Fig. 4B).
537 Expression of the cell division marker *CYCB1;1* was strongly induced in inoculated *aip10-1*
538 mutant plants compared to mock-treated controls, suggesting that the increased DNA
539 replication rates stimulated by beneficial bacterial colonization were followed by higher cell
540 division rates in *aip10-1* plants (Fig. 4C). Overall, increased colonization by PGPB
541 bioinoculants in *aip10-1* mutant plants enhanced the transcriptional regulation of ABAP1 and
542 associated pathway genes, consistent with the greater growth promotion observed following
543 inoculation.

544 Next, based on the RNAseq data from non-inoculated Col-0 and *aip10-1* plants, three
545 genes related to cell wall organization, defense against bacteria, or root hair development were
546 selected for expression analysis in roots under beneficial inoculation, by RT-qPCR (Fig. S1).
547 According to transcriptomic data, LRX*4* was downregulated in *aip10-1* compared to Col-0.
548 This expression pattern was confirmed in mock-treated *aip10-1* plants; however, no additional
549 changes were observed upon bacterial inoculation when compared to wild-type plants (Fig.
550 4D). Similarly, the upregulated expression of *ILA* in *aip10-1* roots identified in the
551 transcriptome analysis was confirmed by RT-qPCR, and similar *ILA* levels were observed in
552 inoculated plants, compared to Col-0 (Fig. 4E). Transcriptomic data revealed upregulation of
553 *RSL4* in *aip10-1* roots. This result was confirmed by RT–qPCR, which showed higher
554 expression levels in mock-treated *aip10-1* plants compared to Col-0, with expression remaining
555 elevated in the presence of both bacterial strains (Fig. 4F). Our analyses showed that gene
556 expression profiles were largely similar between non-inoculated and inoculated *aip10-1* plants,
557 including genes related to cell wall dynamics and bacterial responses.
558 The absence of further transcriptional modulation upon PGPB inoculation suggested
559 that *aip10-1* mutants may already be transcriptionally primed for enhanced association with
560 beneficial plant–microorganism interactions. This genotype appears to provide physiological
561 conditions that favor colonization by beneficial and diazotrophic bacteria, thereby increasing
562 its capacity to respond to their growth-promoting effects.
563

564 **Response of *aip10-1* plants to diazotrophic PGPB inoculation under high and low**
565 **fertilization conditions**

566 Given the enhanced association between *aip10-1* plants and PGPB bioinoculants,
567 together with increased *nifH e*xpression indicating higher nitrogenase activity in inoculated
568 *aip10-1* roots, we investigated whether PGPB inoculation could reduce the dependence of
569 *aip10-1* mutant plants on mineral fertilization. To address this question, inoculation responses
570 of *aip10-1* and Col-0 plants were analyzed under conditions of low and high nutrient
571 availability.
572 The *in vitro* inoculation system was used, followed by greenhouse cultivation under
573 low (0.06 g/L NPK 20:20:20, corresponding to 12 mg/L N, 5.2 mg/L P and 10 mg/L K) and
574 high (0.12 g/L NPK 20:20:20, corresponding to 24 mg/L N, 10.4 mg/L P and 20 mg/L K)
575 nutrient availability. Col-0 and *aip10-1* mutant plants were inoculated with the PGPB *H.*
576 *seropedicae* HRC54, or *G. diazotrophicus* Pal5, or a commercial bioinoculant (Biofree)

577 containing the strains *A. brasilense* Ab-V6 and *P. fluorescens* CCTB03. Four treatment groups
578 were established for both Col-0 and *aip10-1* plants: i) mock-treated plants grown under low
579 fertilization, ii) mock-treated plants grown under high fertilization, iii) plants inoculated with
580 HRC54 or PAL5 or Biofree grown under low fertilization, iv) plants inoculated with HRC54
581 or PAL5 or Biofree grown under high fertilization (Fig. S3). First, root colonization with the
582 PGPB bioinoculants (HRC54 or Pal5 or Biofree) was validated in plants at 7 DAI, before
583 starting differential fertilization treatments, through absolute quantification of a single-copy
584 bacterial gene using genus-specific primers by qPCR (Fig. 3F-G and Fig. S4). Bacterial counts
585 showed that *aip10-1* roots were colonized by a higher number of bacterial cells per gram of
586 plant tissue compared to Col-0, suggesting enhanced interaction between mutant plants and the
587 bioinoculants.

588 The effects of fertilization with high or low doses of nutrients were analyzed in the
589 shoots and roots at 35 DAG (31 DAI) (Fig. 5A and B). Our results showed that *aip10-1* plants
590 were more responsive to bioinoculants under low nutrient availability, exhibiting enhanced
591 growth, like the phenotype observed in mock-treated mutant plants grown under high nutrient
592 availability. In shoot, this beneficial effect was observed through analyses of rosette area and
593 dry biomass, where *aip10-1* inoculated plants presented 22% (HRC54) (Fig. 5C) and 26%
594 (Pal5) (Fig. 5F) larger area, as well as 33% (HRC54) (Fig. 5D) and 35% (Pal5) (Fig. 5G) greater
595 dry weight when grown under low N availability compared to Col-0 plants under the same
596 conditions. Furthermore, rosette area and dry biomass increased by 30% (Fig. 5C and F) and
597 42% (Fig. 5D and G), respectively, in mock-treated *aip10-1* mutant plants under conditions of
598 high nutrient availability. Chlorophyll content analyses demonstrated this same pattern, with
599 an increase in response to both inoculations in *aip10-1* plants compared to wild-type plants
600 under low fertilization conditions (Fig. 5E and H), consistent with the increase observed in
601 mock mutant plants grown under high fertilization, corroborating previous results. Parallel
602 experiments were conducted using a commercial bioinoculant, Biofree (Fig. S4). Under low
603 nutrient availability, *aip10-1* plants inoculated with Biofree exhibited a marked increase in
604 rosette expansion and biomass accumulation compared to mock-treated mutants (Fig. S4).
605 Again, this growth promotion was comparable to that observed in mock-treated *aip10-1* plants
606 grown under high fertilization conditions (Fig. S4).

607 Root phenotypic analyses showed that *aip10-1* plants exhibited more developed root
608 systems in response to inoculation with the HRC54 and Pal5 strains upon low fertilization (Fig.
609 6). Under these conditions, *aip10-1* plants inoculated with HRC54 and Pal5 exhibited 20–51%
610 longer roots (Fig. 6B and E) and 24–42% larger surface area (Fig. 6C and F) compared to Col-

611 0, respectively. At the same time, under high fertilization, non-inoculated *aip10-1* plants still
612 exhibited average increases of 40% in root length and 50% in surface area relative to wild-type
613 plants (Fig. 6B-C and 6E-F). The increased root growth of *aip10-1* mutants resulted in a
614 significant increase in dry biomass. In response to HRC54 and Pal5 inoculation, the gain in
615 root dry weight ranged from 40% (Fig. 6A) to 70% (Fig. 6D) in mutant plants compared to
616 wild-type plants under low fertilization, equivalent to the increase found in *aip10-1* mock-
617 treated plants grown under high fertilization. Under low-nutrient conditions, Biofree
618 inoculation markedly enhanced root biomass, elongation, and surface area in mutant plants,
619 whereas no significant effects were observed in Col-0 (Fig. S5).
620 The use of bioinoculants also promoted growth at the plant reproductive stage (Fig.
621 7A). Consistent with the results for the vegetative phase, low fertilization positively influenced
622 the height of the main inflorescence axis in inoculated mutant plants, in response to both
623 inoculations, compared to Col-0 (Fig. 7B and E). In addition, this combination of stimuli
624 generated inflorescences with 23–29% more siliques on the main axis of inoculated *aip10-1*
625 plants compared to all other groups grown under low fertilization (Fig. 7C and F). Similarly,
626 *aip10-1* mutants produced a higher total seed weight under low fertilization conditions,
627 following inoculation of HRC54 (Fig. 7D) and Pal5 (Fig. 7G). Additionally, the commercial
628 microbial consortium more strongly increased silique number and total seed yield in *aip10-1*
629 than in Col-0, particularly under low nutrient conditions (Fig. S6). Overall, *aip10-1* mutants
630 responded more strongly to bioinoculants containing diazotrophic bacteria, resulting in greater
631 dry biomass accumulation in both shoots and roots compared to Col-0 plants. Moreover, these
632 benefits were primarily evident under low fertilization conditions. Taken together, the results
633 suggest that PGPB bioinoculant application can partially replace mineral fertilization in *aip10-*
634 *1* mutant plants, but not in Col-0, highlighting a genotype-specific response.
635
636 **Nitrogen metabolism in *aip10-1* plants associated with diazotrophic PGPB under high**
637 **and low fertilization conditions**
638 Our data showed that PGPB inoculation in *aip10-1* increased bacterial *nifH* expression
639 and had additive effects on plant biomass and chlorophyl levels. We therefore investigated N
640 assimilation in *aip10-1* plants by analyzing the expression of representatives in two selected
641 key gene families known to respond to changes in N availability and PGPB inoculation
642 (Rosman *et al.*, 2024). The N assimilation genes analyzed were: i) the two Nitrate Reductases
643 (NR) *NIA1* and *NIA2* that are modulated by nitrate availability (Wilkinson and Crawford,
644 1993); ii) and the two Glutamine Synthetase cytosolic genes (GS1), *GLN1;1* and *GLN1;3,* that

645 are high-affinity and low-affinity-related isoforms, respectively (Ishiyama *et al.*, 2004).
646 Analyzes were performed by RT-qPCR of root samples collected at 20 DAG from wild-type
647 and *aip10-1* plants mock-treated or PGPB inoculated and grown in a greenhouse under the high
648 and low fertilization conditions.

649 We first evaluated the N metabolism data in mock-treated plants, as the native
650 microbiome in non-inoculated *aip10-1* root compartment was enriched with PGPB and
651 diazotrophic bacteria. The effects of nutrient availability on *nifH* expression were evaluated in
652 natural microbiomes associated with wild-type and *aip10-1* roots. Consistent with the
653 microbiome data enriched with diazotrophic PGPB, higher *nifH* expression levels were
654 observed in mock-treated *aip10-1* plants grown under low nutrient availability (Fig. 8A).
655 Analysis of nitrogen assimilation pathways showed that *NIA1* and *NIA2* were induced under
656 high nutrients availability in mock-treated *aip10-1* plants (Fig. 8B and C), as was *GLN1;3* (Fig.
657 8E), compared to wild-type Col-0. No modulation of these genes was observed under low
658 nutrients condition. Under both nutritional conditions, mock-treated *aip10-1* plants showed a
659 tendency towards higher levels of *GLN1;1* expression compared to Col-0 (Fig. 8D).

660 Taken together, the data in mock-treated plants showed that the use of high
661 concentration of mineral fertilizers negatively affected the diazotrophic PGPB root microbiome
662 in *aip10-1* roots. However, under these conditions, *AIP10* silencing could activate ammonium
663 and nitrate assimilation pathways, suggesting that *aip10-1* assimilates nitrogen more efficiently
664 compared to wild-type plants. This is consistent with the enhanced biomass accumulation
665 previously reported for *aip10-1* compared to Col-0, growing under high nutrient conditions,
666 further supporting the genotype-specific response.

667 We next evaluated N metabolism in PGPB inoculated plants, as diazotrophic PGPB
668 inoculation of *aip10-1* under low nutrient availability enhanced growth promotion. The control
669 mock-treated Col-0 and *aip10-1* expression data is the same as the one presented in Fig.8. The
670 effects of nutrient availability on *nifH* expression showed that low nutrient availability
671 increased *nifH* expression in *aip10-1* plants inoculated with HRC54 and Pal5 relative to high-
672 nutrient conditions or mock-inoculated controls (Fig. 9A and B). Under low N conditions,
673 *GLN1;1* expression in inoculated *aip10-1* plants showed a tendency toward higher levels,
674 although no significant differences were detected relative to mock controls or to mutant plants
675 grown under high nutrient availability (Fig. 9C and D). In contrast, under low N fertilization,
676 *H. seropedicae* inoculation significantly increased *NIA1* expression in *aip10-1* plants compared
677 to other inoculated groups grown under high or low fertilization, whereas *G. diazotrophicus*
678 inoculation had no effect on *NIA1* expression (Fig. 9E and F). Altogether, these findings

679 suggest that although *nifH* expression was increased in diazotrophic PGPB inoculated *aip10-1*
680 plants, the observed growth promotion may not be explained exclusively by biological N_2
681 fixation. Additional mechanisms may contribute, including PGPB-driven increases in nutrient
682 solubilization and mobilization, nutrient use efficiency (NUE), as well as shifts in the
683 composition of the root-associated microbial community.
684

685 **4. Discussion**

686 Achieving high agricultural productivity while minimizing environmental harm requires
687 the adoption of novel and sustainable approaches that limit dependence on mineral fertilizers.
688 PGPB bioinoculants represent a promising strategy to enhance crop performance while
689 reducing reliance on mineral fertilizers. However, their effectiveness is highly variable and
690 largely depends on plant genetic factors that regulate microbial recruitment and colonization.
691 Although plants actively shape their root-associated microbiota, the molecular mechanisms that
692 enable the accommodation of beneficial PGPB without triggering defense responses,
693 culminating with the promotion of plant growth and yield, remain poorly understood
694 (Vandenkoornhuyse *et al.*, 2015; Zhang *et al.*, 2023). Elucidating these plant-controlled
695 processes is critical for improving the consistency of PGPB-plant interactions.

696 Our research group has systematically investigated the molecular basis of plant-PGPB
697 communication, identifying key plant signaling, transcriptional, and metabolic pathways that
698 are modulated during these interactions ultimately influencing plant physiological and
699 developmental responses (Carvalho *et al.*, 2011, 2016, 2022; Thiebaut *et al.*, 2017; Hardoim *et*
700 *al.*, 2020; Ballesteros *et al.*, 2021; Rosman *et al.*, 2024). Here, we show that among the
701 sugarcane gene networks regulated by inoculation with PGPB is a regulator of cell cycle
702 progression that may modulate plant growth by integrating cell divisions to abiotic and biotic
703 environmental signals. Within this network, AIP10 integrates cell division rates with metabolic
704 regulation, by direct interaction with ABAP, SnRK1 (via KIN10) and possibly additional
705 partners. AIP10 acts as a negative regulator of the cell cycle, and its silencing results in
706 healthier plants with increased biomass and yield, along with enhanced metabolite
707 accumulation, including carbohydrate content (Montessoro *et al.*, 2025). Therefore, we
708 investigated whether *AIP10* silencing contributes to beneficial interactions with PGPB in the
709 endogenous root microbiome or in response do PGPB-bioinoculants, by performing functional
710 analyses in *A. thaliana aip10-1* knockout mutant. Our results showed that the improved
711 performance of *A. thaliana aip10-1* was associated with greater colonization by beneficial
712 bacteria, both within the native root microbiome or following PGPB inoculation. Based on

713 these findings and recent advances in plant–PGPB interactions, we propose potential
714 mechanisms that may explain the enhanced PGPB colonization in *aip10-1*, contributing to the
715 observed increase in plant performance (Figure 10).
716
717 ***AIP10* silencing favored beneficial microbial recruitment**
718 Increasing evidence suggests that plant performance and environmental adaptation rely
719 on coordinated interactions with the root microbiota. Data are emerging showing that genes
720 governing development, immune responses, nutrient uptake, and metabolite release can
721 possibly function as determinants of the microbiome assembly (Zhang *et al.*, 2023).
722 Consistently, we found that the loss of *AIP10* function in *A. thaliana* reshaped root-associated
723 bacterial communities while maintaining a substantial core of shared taxa. Notably, *aip10-1*
724 plants preferentially recruited beneficial PGPB, particularly diazotrophic species, in both the
725 root compartment and rhizospheric soil, while being depleted in potentially pathogenic taxa.
726 The mechanisms by which *aip10-1* re-shapes its root microbiome may involve
727 alterations in plant carbohydrate metabolism, reported as key nutrient sources for PGPB
728 (Upadhyay *et al.*, 2022; Hemelda and Noutoshi, 2025). Carbohydrate levels were quantitatively
729 increased in *aip10-1* plants indicating changes in primary metabolism (Montessoro *et al.*,
730 2025). Consistently, genes associated with carbohydrate metabolic pathways were found as
731 differentially expressed in *aip10* roots, suggesting that altered carbon availability could support
732 the recruitment of diazotrophic PGPB. Root-derived metabolites were also shown to play an
733 actively selective role in shaping the root microbiome, as mutant in genes involved in
734 regulating specialized metabolites influenced microbial recruitment, community structure, and
735 function (Vandenkoornhuyse *et al.*, 2015; Zhang *et al.*, 2023). Loss-of-function mutations in
736 genes controlling coumarin biosynthesis or export significantly modified rhizosphere and
737 endosphere communities, promoting the recruitment of growth-promoting or nutrient-
738 mobilizing bacteria through changes in root-derived specialized metabolites (Stringlis *et al.*,
739 2018; Huang *et al.*, 2019; Voges *et al.*, 2019). Secondary metabolites such as phenolics and
740 terpenes have been shown to modulate microbiome composition and enrich beneficial taxa
741 (Stringlis *et al.*, 2018; Harbort *et al.*, 2020). Furthermore, genotype-specific metabolites
742 explain substantial microbiome variation in crops such as rice (Liu *et al.*, 2025).
743 In parallel, in rice, NRT1.1B, a nitrate transporter and sensor, was associated with
744 modulation of root microbiota composition, integrated with higher NUE in field-grown plants
745 (Zhang *et al.*, 2019). Consistent with this mechanism, non-inoculated *aip10-1* plants showed

746 higher expression of N assimilation genes compared to Col-0, along with a root microbiota
747 enriched in PGPB and diazotrophic bacteria that enhance N availability to the plant.
748 *aip10-1* mutants showed transcriptional reprogramming of genes in pathways related
749 to plant-microorganism interaction such as cell wall formation, hormonal responses, defense
750 and immune response to bacteria. In *aip10-1* roots, induction of genes involved in cell wall
751 loosening, such as *XTH* and *PME46*, and repression of genes associated with cell wall
752 reinforcement and stress-related remodeling, including *EXT15* and *LRX3,* suggest increased
753 cell wall plasticity. This shift may facilitate bacterial association and root tissue colonization.
754 In sugarcane, genotypes that efficiently associate with endophytic diazotrophic bacteria show
755 extensive reprogramming of cell wall–modifying genes, promoting increased tissue plasticity
756 and microbial accommodation (Ballesteros *et al.*, 2021). Consistent with this, broader evidence
757 indicates that cell wall remodeling is a key feature of plant readiness for symbiotic or
758 associative interactions, as exposure to PGPR commonly induces expansins and XTHs across
759 diverse plant species (Vacheron *et al.*, 2013; Srivastava *et al.*, 2023).
760 Alterations in innate immunity pathways may also lead to distinctive microbial
761 assemblages, as shown in mutants impaired in pattern-recognition receptors, which exhibit
762 shifts in core bacterial taxa and increased abundance of taxa typically associated with beneficial
763 functions (Ma *et al.*, 2021). In *aip10-1* roots, some genes involved in immune and defense
764 pathways related to bacterial interactions were either repressed or induced. Such transcriptional
765 reprogramming is required for successful beneficial associations with PGPB, as plants must
766 downregulate specific defense responses to permit bacterial colonization while simultaneously
767 activating other defense pathways to prevent bacterial overgrowth (Carvalho *et al.*, 2016).
768 Furthermore, it might participate in the regulation how roots perceive and respond to soil
769 microorganisms, creating a more permissive environment for colonization by diazotrophic and
770 PGPB-enriched taxa while limiting the presence of potential pathogens. Upregulation of
771 bacterial response regulators such as ILA in *aip10-1* is consistent with plants genetically
772 primed for beneficial microbial associations showing enhanced sensitivity to microbe-derived
773 signals before colonization (Liu *et al.*, 2017; Gao *et al.*, 2022).
774 The transcriptional profile of *aip10-1* plants in the absence of PGPB inoculation
775 resembles signatures reported in plant genotypes with enhanced capacity to interact with
776 beneficial microorganisms. It suggests that *AIP10* silencing may induce a primed physiological
777 state that facilitates the establishment of growth-promoting associations with PGPB.
778

Enhanced growth promotion in *aip10-1* in response to PGPB inoculation were driven by cell division and nutrient availability

Our data suggest that mock *aip10-1* genotype is primed for enhanced association with PGPB bioinoculants. This genotype appears to provide physiological conditions that favor colonization by beneficial and diazotrophic bacteria, thereby increasing plant's capacity to respond to their growth-promoting effects. Consistent with a native root microbiota enriched with beneficial bacteria, inoculated *aip10-1* genotype was colonized by higher numbers of PGPB bioinoculant during early phases after inoculation. Consequently, *aip10-1* plants exhibited increased root and shoot dry biomass and higher productivity in response to inoculation with distinct PGPB, such as *G. diazotrophicus* Pal5, *H. seropedicae* HRC54, and Biofree, compared to inoculated wild-type plants. Moreover, the enhanced traits observed in non-inoculated *aip10-1* plants were further amplified upon inoculation, indicating additive effects on plant growth promotion.

Increased plant dry biomass ultimately depends on higher rates of cell division, as plant growth and morphogenesis are governed by the balance between cell division, cell expansion, and cell differentiation (Hemerly et al. 1999, Jorgensen and Tyers, 2004; Jones *et al.*, 2017; Carneiro *et al.*, 2021). AIP10 is part of a regulatory network that controls plant growth by modulating cell cycle progression at G1 to S phase, a key checkpoint regulated by environmental signals, such as biotic interactions (Masuda *et al.*, 2008; Montessoro *et al.*, 2025). ABAP1 and AIP10 negatively regulate DNA replication by reducing the activity of the pre-replication complex (preRC) and by decreasing transcription of preRC members as *AtCdt1a* and *AtCdt1b* (Masuda *et al.*, 2008; Montessoro *et al.,* 2025). In addition, *ABAP1* expression is reduced in *aip10-1* plants suggesting that AIP10 may also control cell division through a feedback mechanism of *ABAP1* transcriptional control. Our results suggest that the enhanced growth of *aip10-1* plants in response to bioinoculants can be increased by the negative regulation of *ABAP1*, favoring higher cell division rates and increased growth. Moreover, *AtCDT1a* showed increased expression in *aip10-1* plants after inoculation with both bioinoculants. A similar pattern was observed for the cell division marker *CYCB1;1*, supporting the idea that beneficial bacterial colonization could stimulate higher cell division rates in *aip10-1*.

PGPB associations can promote plant growth and increase dry biomass through mechanisms that enhance nutrient availability such as biological nitrogen fixation and mineral solubilization, and by improvement of nutrient use efficiency (Thiebaut *et al.*, 2022). Here, we showed that nutrient availability modulated the interaction between PGPB and *aip10-1* plants,

813 with an intensified growth-promoting response under low-fertilization conditions. PGPB
814 inoculation in low nutrient availability resulted in enhanced growth similar to that observed in
815 non-inoculated mutant plants grown under high fertilization (Montessoro *et al.*, 2025). Under
816 these conditions, inoculation increased shoot biomass accumulation by up to 35% in *aip10-1*
817 plants under low fertilization. Silencing *AIP10* promoted the formation of more robust root
818 systems in response to inoculation with HRC54 and Pal5 under low fertilization, increasing
819 root surface area by up to 42% compared to Col-0. This enhanced root growth resulted in a
820 significant increase in dry biomass, with gains of up to 70% after inoculation, equivalent to the
821 increase observed in non-inoculated *aip10-1* plants grown under high fertilization.

822 N levels in the environment regulate the expression of multiple genes involved in
823 assimilation, transport, and utilization (Wilkinson and Crawford, 1993; Lothier *et al.*, 2011;
824 O'Brien *et al.*, 2016). In this study, we investigated the expression pattern of members of GS
825 and NR gene families, which regulate N assimilation and are modulated by variations in N
826 availability, particularly in the presence of PGPB (Rosman *et al.*, 2024). High nutrient
827 availability induced the expression of *NIA1*, *NIA2*, and *GLN1;3*, in mock-treated aip*10-1* plants
828 compared to wild-type plants, with no additional effect of inoculation. Under low fertilization
829 conditions, *NIA1* was induced in *H. seropedicae* inoculated *aip10-1.* Transcriptome analysis
830 revealed that *NIA1* was induced in shoots and roots of *A. thaliana* in response to inoculation
831 with Pal5, at 50 DAI (Soares *et al.*, 2024). Moreover, inoculation with the endophytic fungus
832 *Piriformospora indica* induced NR gene expression, resulting in increased N accumulation in
833 *A. thaliana* and tobacco seedlings (Sherameti *et al.*, 2005).

834 From the bacterial perspective, *nifH* expression in HRC54 and PAL5 inoculated *aip10-*
835 *1* plants was consistently higher compared to Col-0 for both strains at 7 DAI. Remarkably, this
836 difference persisted at 16 DAI only under low-nutrient conditions. Given that the plant growth-
837 promoting capacity of *H. seropedicae* and *G.* relies on coordinated N_2-fixation–related gene
838 activity (Pedrosa *et al.*, 2011; Tufail *et al.*, 2021), our results suggest that *AIP10* loss of function
839 of *AIP10* not only enhances root colonization by PGPB, but also potentiates bacterial N_2-
840 fixation metabolism, especially in environments with low N availability.

841 The efficiency of the interaction between plants and PGPB has been widely attributed
842 to external conditions, including plant genotype, bacterial genotype, and soil nutrient
843 availability (Ballesteros *et al.*, 2021; Carvalho *et al.*, 2022; Rosman *et al.*, 2024). Among these
844 factors, the nutritional composition of the soil stands out, playing an essential role in controlling
845 plant growth and development, including the establishment of the plant-PGPB association.

Low N fertilization conditions encourage the establishment of efficient plant-bacteria associations (Tufail *et al.*, 2021; Rosman *et al.*, 2024).

In sugarcane, the association with PGPB can contribute up to 70% of all accumulated N through BNF or improved NUE, varying according to the plant and bacterial genotype and soil fertility (Urquiaga *et al.*, 2012; Antunes *et al.*, 2019; Martins *et al.*, 2020; Singh *et al.*, 2021). Among the diazotrophic bacteria that are associated with sugarcane, the *Herbaspirillum* stands out, found colonizing the apoplast of leaves, very close to the vascular parenchyma cells (Silva *et al.*, 2003). Several studies have already reported the positive effects of this association, such as promoting increased biomass, shoot and secondary root growth, as well as the accumulation of N, P and K (Oliveira *et al.*, 2006; dos Santos *et al.*, 2020; Martins *et al.*, 2020). Specifically for *H. seropedicae* in maize, inoculation has been shown to increase root fresh mass, root surface area (Nunes *et al.*, 2021); number of lateral roots (Do Amaral *et al.*, 2014; Ferrari *et al.*, 2014; Hardoim *et al.*, 2020); N accumulation (Brusamarello-Santos *et al.*, 2017); in addition to altering N metabolism and ensuring tolerance to abiotic stresses (Alves *et al.*, 2014; Curá *et al.*, 2017; Breda *et al.*, 2019; Dias *et al.*, 2021). Moreover, *aip10-1* plants inoculated with Biofree showed increased rosette expansion and biomass accumulation compared with mock-treated mutants under low nutrient availability. As this commercial bioinoculant comprises *A. brasilense* Ab-V6 and *P. fluorescens* CCTB03, PGPB associated with phytohormone synthesis and phosphate solubilization (Park *et al.*, 2009; Zhao *et al.*, 2025), these results suggest that multiple growth-promoting mechanisms may contribute to enhanced plant performance in plants with silenced *AIP10* expression under reduced chemical fertilization.

AIP10 as a regulatory target for improving plant performance under nutrient-limited conditions in association with PGPB

Conventional strategies for maintaining high crop productivity largely depend on the extensive application of nitrogen-based fertilizers. However, crop yields have not increased proportionally to fertilizer inputs, revealing low NUE and higher production costs (Mueller *et al.*, 2019). In this context, to meet the nutritional needs of crops and maintain high levels of productivity, modern agriculture has resorted to the use of bio-inputs, which favor plant production, soil health, and the reduction of GHG emissions. Therefore, investing in alternatives such as modulation of native root microbiomes to favor enrichment with PGPB, or development PGPB-based biological inputs, becomes crucial strategies to ensure the

879 agricultural sustainability of various crops such as maize, sugarcane, wheat, and rice (Canellas
880 *et al.*, 2013; Martins *et al.*, 2020; Carril *et al.*, 2021; Pankievicz *et al.*, 2021; Tufail *et al.*, 2021).
881 Dissecting the plant genetic factors that govern the attraction of beneficial PGPB within the
882 microbiome, as well as the establishment of effective interactions with PGPB bioinoculants, is
883 essential for improving crop yield and plant fitness.

884 The absence of AIP10 shaped root microbiome to a higher abundance of PGPB and
885 diazotrophic bacteria. This technology also increased responsiveness to colonization by
886 bioinoculants under low nutrient availability. Remarkably, the enhanced traits observed in non-
887 inoculated *aip10-1* plants were further amplified upon inoculation, indicating additive effects
888 on plant growth promotion. Our observations raise the important question of why the loss of
889 AIP10 function, a gene conserved across terrestrial plants, confer advantages such as enhanced
890 root colonization by beneficial bacteria. Loss of AIP10 activity confers traits associated with
891 enhanced terrestrial resilience, including increased CO_2 assimilation, reduced transpiration, and
892 improved water-use efficiency. We therefore hypothesize that AIP10 contributes to the
893 regulation of soil–microbe interactions as part of plant adaptation to terrestrial environments.

894 Here, we investigated the modulation of the native root microbiome and the response
895 to bioinoculant inoculation in *A. thaliana aip10-1* plants, aiming to enhance plant growth and
896 biomass accumulation under reduced chemical fertilization. Under low fertilization conditions,
897 plants lacking AIP10 shaped their root microbiome toward a higher abundance of PGPB and
898 diazotrophic bacteria and displayed improved responsiveness to bioinoculants, accumulating
899 biomass comparable to that of non-inoculated plants grown under high fertilization. In addition,
900 similarly to the vegetative phase, low fertilization increased reproductive development, leading
901 to a 29% increase in siliques on the main inflorescence axis compared with all other groups
902 under the same conditions. Taken together, our results indicate that modifying *AIP10*
903 expression, previously associated with the control of a central hub that integrates cell division
904 rates and primary metabolism, can be used as a strategy to improve nutrient use efficiency
905 under low chemical fertilization, contributing to a more sustainable and regenerative
906 agriculture. This approach results in a real increase in biomass, productivity, and possibly the
907 nutritional value of the plants, having an important impact on food security.

908 **Supplementary data**

909 The following supplementary data are available at JWB online.

910 Supplementary Table S1. Primers used in this study.

911 Supplementary Table S2. Relative abundance of diazotrophic, plant growth–promoting
912 (PGPB), and pathogenic bacterial communities associated with the roots of Col-0 and *aip10-1*
913 plants.

914 Supplementary Fig. S1. Differential gene expression patterns in Col-0 and *aip10-1* roots of *A.*
915 *thaliana* 11 days after germination.

916 Supplementary Fig S2. Visualization of bacterial colonization patterns in different root zones
917 of *A. thaliana* Col-0 and *aip10-1* mutant plants.

918 Supplementary Fig S3. Experimental design of the differential fertilization trial in *aip10-1* and
919 wild-type Col-0 plants inoculated with *H. seropedicae* HRC54 (HRC54), *G. diazotrophicus*
920 Pal5 (Pal5), Biofree or non-inoculated (mock).

921 Supplementary Fig S4. Growth performance and physiological responses of Col-0 and *aip10-*
922 *1* plants inoculated with commercial bioinoculant Biofree under contrasting nutrient
923 conditions.

924 Supplementary Fig S5. Root architecture responses of Col-0 and *aip10-1 A. thaliana* plants to
925 Biofree inoculation under contrasting nutrient conditions.

926 Supplementary Fig S6. Reproductive performance of Col-0 and *aip10-1 A. thaliana* plants in
927 response to Biofree inoculation under high- and low-nutrient conditions.

928 **Author contribution**

929 MCU: Data curation, Investigation, Methodology, Writing – original draft, Writing – review
930 & editing. HF: Data curation, Investigation, Methodology, Writing – original draft, Writing –
931 review & editing. PM: Data curation, Methodology, Writing – original draft. JVS:
932 Methodology, Writing – original draft. SGE: Data curation, Methodology, AH: Funding
933 acquisition, Supervision, Writing – review & editing.

934 **Conflict of interest**

935 The authors declare that there is no conflict of interest.

936 **Funding**

This research was supported by grants from Fundação de Amparo a Pesquisa do Estado do Rio de Janeiro (FAPERJ) and Conselho Nacional de Desenvolvimento Científico e Tecnológico (CNPq). CNPq, FAPERJ, and the Coordination for the Improvement of Higher Education Personnel (CAPES) also supported the work with graduate and post-graduate scholarships. MCU and HF were supported by a CNPq postdoctoral fellowship. PM were supported by CNPq/SEMPI/MCTI grant no. 021/2021 (Rhae Program). SGE was supported by a CAPES MSc fellowship. JVS was supported by a CNPq undergraduate fellowship. ASH was supported by a research scientist fellowship from CNPq (306643/2022-7).

5. References

Alves GC, Videira SS, Urquiaga S, Reis VM. 2014. Differential plant growth promotion and nitrogen fixation in two genotypes of maize by several Herbaspirillum inoculants. Plant Soil, 1–15.

Do Amaral FP, Bueno JCF, Hermes VS, Arisi ACM. 2014. Gene expression analysis of maize seedlings (DKB240 variety) inoculated with plant growth promoting bacterium Herbaspirillum seropedicae. Symbiosis **62**, 41–50.

Antunes JEL, De Freitas ADS, Oliveira LMS, De Lyra MDCCP, Fonseca MAC, Santos CERS, De Oliveira JP, De Araújo ASF, Figueiredo MVB. 2019. Sugarcane inoculated with endophytic diazotrophic bacteria: Effects on yield, biological nitrogen fixation and industrial characteristics. Anais da Academia Brasileira de Ciencias **91**, 1–12.

Aquino JPA, Antunes JEL, Bonifácio A, Rocha SMB, Amorim MR, Alcântara Neto F, Araujo ASF. 2021. Plant growth-promoting bacteria improve growth and nitrogen metabolism in maize and sorghum. Theoretical and Experimental Plant Physiology **33**, 249–260.

Baldani JI, Pot B, Kirchhof G, *et al.* 1996. Emended Description of Herbaspirillum; Inclusion of [Pseudomonas] rubrisubalbicans, a Mild Plant Pathogen, as Herbaspirillum rubrisubalbicans comb. nov.; and Classification of a Group of Clinical Isolates (EF Group 1) as Herbaspirillum Species 3. International Journal of Systematic Bacteriology, 802–810.

Ballesteros HGF, Rosman AC, Carvalho TLG, Grativol C, Hemerly AS. 2021. Cell wall formation pathways are differentially regulated in sugarcane contrasting genotypes associated with endophytic diazotrophic bacteria. Planta **254**, 1–21.

Bauhus J, Messier C. 1999. IMAGE ANALYSIS Evaluation of Fine Root Length and Diameter Measurements Obtained Using RHIZO Image Analysis. Agronomie **91**, 142–147.

Breda FA, da Silva TFR, dos Santos SG, Alves GC, Reis VM. 2019. Modulation of nitrogen metabolism of maize plants inoculated with Azospirillum brasilense and Herbaspirillum seropedicae. Archives of Microbiology **201**, 547–558.

Brusamarello-Santos LC, Gilard F, Brulé L, Quilleré I, Gourion B, Ratet P, De Souza EM, Lea PJ, Hirel B. 2017. Metabolic profiling of two maize (Zea mays L.) inbred lines inoculated with the nitrogen fixing plant-interacting bacteria Herbaspirillum seropedicae and Azospirillum brasilense. PLoS ONE **12**, 1–19.

Canellas LP, Balmori DM, Médici LO, Aguiar NO, Campostrini E, Rosa RCC, Façanha AR, Olivares FL. 2013. A combination of humic substances and Herbaspirillum seropedicae inoculation enhances the growth of maize (Zea mays L.). Plant and Soil **366**, 119–132.
Carneiro AK, Montessoro P da F, Fusaro AF, Araújo BG, Hemerly AS. 2021. Plant cdks—driving the cell cycle through climate change. Plants **10**, 1–27.
Carril P, Cruz J, di Serio C, Pieraccini G, Ait Bessai S, Tenreiro R, Cruz C. 2021. Modulation of the Wheat Seed-Borne Bacterial Community by Herbaspirillum seropedicae RAM10 and Its Potential Effects for Tryptophan Metabolism in the Root Endosphere. Frontiers in Microbiology **12**.
Carvalho T, Ballesteros H, Thiebaut F, Ferreira P, Hemerly A. 2016. Nice to meet you: genetic, epigenetic and metabolic controls of plant perception of beneficial associative and endophytic diazotrophic bacteria in non-leguminous plants. Plant Molecular Biology **90**, 1–14.
Carvalho TLG, Balsemão-Pires E, Saraiva RM, Ferreira PCG, Hemerly AS. 2014. Nitrogen signalling in plant interactions with associative and endophytic diazotrophic bacteria. Journal of Experimental Botany **65**, 5631–5642.
Carvalho TLG, Ferreira PCG, Hemerly AS. 2011. Sugarcane Genetic Controls Involved in the Association with Beneficial Endophytic Nitrogen Fixing Bacteria. Tropical Plant Biology **4**, 31–41.
Carvalho TLG, Rosman AC, Grativol C, Nogueira EM, Baldani J, Hemerly AS. 2022. Sugarcane Genotypes with Contrasting Biological Nitrogen Fixation Efficiencies Differentially Modulate Nitrogen. Plants **11**, 1–31.
Cohen AC, Bottini R, Pontin M, Berli FJ, Moreno D, Boccanlandro H, Travaglia CN, Piccoli PN. 2015. Azospirillum brasilense ameliorates the response of Arabidopsis thaliana to drought mainly via enhancement of ABA levels. Physiologia Plantarum **153**, 79–90.
Curá A, Franz DR, Filosofía JE, Balestrasse KB, Burgueño LE. 2017. Inoculation with Azospirillum sp . and Herbaspirillum sp . Bacteria Increases the Tolerance of Maize to Drought Stress. Microorganisms, 1–16.
Dias AC, Alves GC, Da Silva TFR, Alves BJR, Santos LA, Reis VM. 2021. Comparison of N uptake of maize inoculated with two diazotrophic bacterial species grown under two N levels. Archives of Agronomy and Soil Science **00**, 1–17.
Dora S, Terrett OM, Sánchez-Rodríguez C. 2022. Plant-microbe interactions in the apoplast: Communication at the plant cell wall. Plant Cell **34**, 1532–1550.
Doyle JJ, Doyle JL. 1987. A Rapid DNA Isolation Procedure for Small Quantities of Fresh Leaf Tissue. Phytochemical Bulletin **19**, 11–15.
Draeger C, Ndinyanka Fabrice T, Gineau E, *et al.* 2015. Arabidopsis leucine-rich repeat extensin (LRX) proteins modify cell wall composition and influence plant growth. BMC Plant Biology **15**, 1–11.
Espindula E, Sperb ER, Bach E, Passaglia LMP. 2019. The combined analysis as the best strategy for dual RNA-seq mapping. Genetics and Molecular Biology **42**.
Faus I, Niñoles R, Kesari V, Llabata P, Tam E, Nebauer SG, Santiago J, Hauser MT, Gadea J. 2018. Arabidopsis ILITHYIA protein is necessary for proper chloroplast biogenesis and root development independent of eIF2α phosphorylation. Journal of Plant Physiology **224–225**, 173–182.

Favero VO, Carvalho RH, Motta VM, Leite ABC, Coelho MRR, Xavier GR, Rumjanek NG, Urquiaga S. 2021. Bradyrhizobium as the Only Rhizobial Inhabitant of Mung Bean (Vigna radiata) Nodules in Tropical Soils: A Strategy Based on Microbiome for Improving Biological Nitrogen Fixation Using Bio-Products. Frontiers in Plant Science **11**, 1–16.
Ferrarezi JA, Carvalho-Estrada P de A, Batista BD, *et al.* 2022. Effects of inoculation with plant growth-promoting rhizobacteria from the Brazilian Amazon on the bacterial community associated with maize in field. Applied Soil Ecology **170**, 1–14.
Ferrari CS, Amaral FP, Bueno JCF, Scariot MC, Valentim-Neto PA, Arisi ACM. 2014. Expressed Proteins of Herbaspirillum seropedicae in Maize (DKB240) Roots-Bacteria Interaction Revealed Using Proteomics. Applied Biochemistry and Biotechnology **174**, 2267–2277.
Filgueiras L, Silva R, Almeida I, Vidal M, Baldani JI, Meneses CHSG. 2020. Gluconacetobacter diazotrophicus mitigates drought stress in Oryza sativa L. Plant and Soil **451**, 57–73.
Fukami J, Ollero FJ, Megías M, Hungria M. 2017. Phytohormones and induction of plant-stress tolerance and defense genes by seed and foliar inoculation with Azospirillum brasilense cells and metabolites promote maize growth. AMB Express **7**, 1–13.
Gao Y, Feng J, Wu J, Wang K, Wu S, Liu H, Jiang M. 2022. Transcriptome analysis of the growth-promoting effect of volatile organic compounds produced by Microbacterium aurantiacum GX14001 on tobacco (Nicotiana benthamiana). BMC Plant Biology **22**, 1–15.
Govindasamy P, Muthusamy SK, Bagavathiannan M, *et al.* 2023. Nitrogen use efficiency—a key to enhance crop productivity under a changing climate. Frontiers in Plant Science **14**, 1–48.
Harbort CJ, Hashimoto M, Inoue H, *et al.* 2020. Root-Secreted Coumarins and the Microbiota Interact to Improve Iron Nutrition in Arabidopsis. Cell Host and Microbe **28**, 825-837.e6.
Hardoim PR, de Carvalho TLG, Ballesteros HGF, Bellieny-Rabelo D, Rojas CA, Venancio TM, Ferreira PCG, Hemerly AS. 2020. Genome-wide transcriptome profiling provides insights into the responses of maize (Zea mays L.) to diazotrophic bacteria. Plant and Soil **451**, 121–143.
Hemelda NM, Noutoshi Y. 2025. Root-exuded sugars as drivers of rhizosphere microbiome assembly. Plant Biotechnology **42**, 215–227.
Huang AC, Jiang T, Liu YX, Bai YC, Reed J, Qu B, Goossens A, Nützmann HW, Bai Y, Osbourn A. 2019. A specialized metabolic network selectively modulates Arabidopsis root microbiota. Science **364**, 1–11.
Ishiyama K, Inoue E, Watanabe-Takahashi A, Obara M, Yamaya T, Takahashi H. 2004. Kinetic Properties and Ammonium-dependent Regulation of Cytosolic Isoenzymes of Glutamine Synthetase in Arabidopsis. Journal of Biological Chemistry **279**, 16598–16605.
Jones AR, Forero-Vargas M, Withers SP, Smith RS, Traas J, Dewitte W, Murray JAH. 2017. Cell-size dependent progression of the cell cycle creates homeostasis and flexibility of plant cell size. Nature Communications **8**, 1–13.
Jorgensen P, Tyers M. 2004. How cells coordinate growth and division. Current Biology **14**, 1–14.

Kandel SL, Joubert PM, Doty SL. 2017. Bacterial endophyte colonization and distribution within plants. Microorganisms **5**.
Konishi N, Saito M, Imagawa F, Kanno K, Yamaya T, Kojima S. 2018. Cytosolic Glutamine Synthetase Isozymes Play Redundant Roles in Ammonium Assimilation under Low-Ammonium Conditions in Roots of Arabidopsis thaliana. Plant and Cell Physiology **59**, 601–613.
Leandro MR, Rangel PL, dos Santos TC, *et al.* 2019. Colonization of Arabidopsis thaliana by Herbaspirillum seropedicae promotes its growth and changes its proteomic profile. Plant and Soil **443**, 429–447.
Lebeis SL, Sur Herrera Paredes, Derek S. Lundberg, *et al.* 2015. Salicylic acid modulates colonizationof the root microbiome by specificbacterial taxa. Science **349**, 860–864.
Liu H, Carvalhais LC, Crawford M, Singh E, Dennis PG, Pieterse CMJ, Schenk PM. 2017. Inner plant values: Diversity, colonization and benefits from endophytic bacteria. Frontiers in Microbiology **8**, 1–17.
Liu Y, Xu C, Chen S, Chu G, Yu K, Wang D. 2025. Beyond genotype: the influence of developmental stage on rice rhizospheric microbiome-metabolome networks. BMC Plant Biology **25**.
Logemann J, Schell J, Willmitzer L. 1987. Improved Method for the Isolation of RNA from Plant Tissues. ANALYTICAL BIOCHEMISTRY **163**, 16–20.
Lothier J, Gaufichon L, Sormani R, Lemaître T, Azzopardi M, Morin H, Chardon F, Reisdorf-Cren M, Avice JC, Masclaux-Daubresse C. 2011. The cytosolic glutamine synthetase GLN1;2 plays a role in the control of plant growth and ammonium homeostasis in Arabidopsis rosettes when nitrate supply is not limiting. Journal of Experimental Botany **62**, 1375–1390.
Ma KW, Niu Y, Jia Y, *et al.* 2021. Coordination of microbe–host homeostasis by crosstalk with plant innate immunity. Nature Plants **7**, 814–825.
Martins DS, Reis VM, Schultz N, Alves BJR, Urquiaga S, Pereira W, Sousa JS, Boddey RM. 2020. Both the contribution of soil nitrogen and of biological N2 fixation to sugarcane can increase with the inoculation of diazotrophic bacteria. Plant and Soil **454**, 155–169.
Masuda HP, Cabral LM, De Veylder L, Tanurdzic M, De Almeida Engler J, Geelen D, Inzé D, Martienssen RA, Ferreira PCG, Hemerly AS. 2008. ABAP1 is a novel plant Armadillo BTB protein involved in DNA replication and transcription. EMBO Journal **27**, 2746–2756.
Monaghan J, Li X. 2010. The HEAT repeat protein ILITYHIA is Required for plant immunity. Plant and Cell Physiology **51**, 742–753.
Montessoro P, Paixão JFR, Costa CNM, *et al.* 2025. The ABAP1 interacting protein 10 (AIP10) exerts a dual role in the cell cycle and primary metabolism pathways in Arabidopis thaliana. Plant Journal **123**, 1–24.
Moretti LG, Crusciol CAC, Bossolani JW, Calonego JC, Moreira A, Garcia A, Momesso L, Kuramae EE, Hungria M. 2021. Beneficial microbial species and metabolites alleviate soybean oxidative damage and increase grain yield during short dry spells. European Journal of Agronomy **127**, 1–12.
Mueller SM, Messina CD, Vyn TJ. 2019. Simultaneous gains in grain yield and nitrogen efficiency over 70 years of maize genetic improvement. Scientific Reports **9**, 1–8.

Nichio BT de L, Chaves RBR, Pedrosa F de O, Raittz RT. 2025. Exploring diazotrophic diversity: unveiling Nif core distribution and evolutionary patterns in nitrogen-fixing organisms. BMC Genomics **26**, 1–17.
Nunes R de O, Domiciano Abrahão G, de Sousa Alves W, Aparecida de Oliveira J, César Sousa Nogueira F, Pasqualoto Canellas L, Lopes Olivares F, Benedeta Zingali R, Soares MR. 2021. Quantitative proteomic analysis reveals altered enzyme expression profile in Zea mays roots during the early stages of colonization by Herbaspirillum seropedicae. Proteomics **21**, 1–12.
O'Brien JAA, Vega A, Bouguyon E, Krouk G, Gojon A, Coruzzi G, Gutiérrez RAA. 2016. Nitrate Transport, Sensing, and Responses in Plants. Molecular Plant **9**, 837–856.
Oliveira LM De, Canuto EDL, Urquiaga S, Reis VM. 2006. Yield of micropropagated sugarcane varieties in different soil types following inoculation with diazotrophic bacteria. **1**, 23–32.
Omara P, Aula L, Oyebiyi F, Raun WR. 2019. World Cereal Nitrogen Use Efficiency Trends: Review and Current Knowledge. Agrosystems, Geosciences and Environment **2**, 1–8.
Orozco-Mosqueda M del C, Santoyo G, Glick BR. 2023. Recent Advances in the Bacterial Phytohormone Modulation of Plant Growth. Plants **12**, 1–15.
Pankievicz VC, do Amaral FP, Ané JM, Stacey G. 2021. Diazotrophic bacteria and their mechanisms to interact and benefit cereals. Molecular Plant-Microbe Interactions **34**, 491–498.
Park KH, Lee CY, Son HJ. 2009. Mechanism of insoluble phosphate solubilization by Pseudomonas fluorescens RAF15 isolated from ginseng rhizosphere and its plant growth-promoting activities. Letters in Applied Microbiology **49**, 222–228.
Pedrosa FO, Monteiro RA, Wassem R, *et al.* 2011. Genome of herbaspirillum seropedicae strain SmR1, a specialized diazotrophic endophyte of tropical grasses. PLoS Genetics **7**, 1–10.
Pereira W, Oliveira RP, Pereira A, Sousa JS, Schultz N, Urquiaga S, Reis VM. 2021. Nitrogen acquisition and 15N-fertiliser recovery efficiency of sugarcane cultivar RB92579 inoculated with five diazotrophs. Nutrient Cycling in Agroecosystems **119**, 37–50.
Pierik R, Fankhauser C, Strader LC, Sinha N. 2021. Architecture and plasticity: Optimizing plant performance in dynamic environments. Plant Physiology **187**, 1029–1032.
Qi F, Zhang F. 2020. Cell cycle regulation in the plant response to stress. Frontiers in Plant Science **10**, 1–23.
Rodrigues GL, Matteoli FP, Gazara RK, *et al.* 2022. Characterization of cellular, biochemical and genomic features of the diazotrophic plant growth-promoting bacterium Azospirillum sp. UENF-412522, a novel member of the Azospirillum genus. Microbiological Research **254**, 1–12.
Rosman AC, Urquiaga MC de O, Thiebaut F, Ballesteros HGF, de Oliveira EAG, Hemerly AS. 2024. Dual RNA-seq of maize and H. seropedicae ZAE94 association, in different doses of nitrate, reveals novel insights into Plant-PGPB-environment relationship. Frontiers in Plant Science **15**, 1–23.
Di Salvo LP, Cellucci GC, Carlino ME, García de Salamone IE. 2018. Plant growth-promoting rhizobacteria inoculation and nitrogen fertilization increase maize (Zea mays L.)

grain yield and modified rhizosphere microbial communities. Applied Soil Ecology **126**, 113–120.
dos Santos R, Andrea P, Diaz E, Lana L, Lobo B. 2020. Use of Plant Growth-Promoting Rhizobacteria in Maize and Sugarcane : Characteristics and Applications. **4**, 1–15.
Dos Santos TC, Leandro MR, Maia CY, Rangel P, Soares FS, Reis R, Passamani L, Silveira V, De Souza Filho GA. 2020. Arabidopsis thaliana exudates induce growth and proteomic changes in Gluconacetobacter diazotrophicus. PeerJ **8**.
Schindelin J, Arganda-Carreras I, Frise E, *et al.* 2012. Fiji: An open-source platform for biological-image analysis. Nature Methods **9**, 676–682.
Sherameti I, Shahollari B, Venus Y, Altschmied L, Varma A, Oelmüller R. 2005. The endophytic fungus Piriformospora indica stimulates the expression of nitrate reductase and the starch-degrading enzyme glucan-water dikinase in tobacco and Arabidopsis roots through a homeodomain transcription factor that binds to a conserved motif in their promoters. Journal of Biological Chemistry **280**, 26241–26247.
Silva GL, Miguens CF, Olivares FL. 2003. Herbaspirillum seropedicae and sugarcane endophytic interaction investigated by using high pressure freezing electron microscopy. Brazilian Journal of Microbiology **34**, 69–71.
Singh P, Singh RK, Li HB, *et al.* 2021. Diazotrophic Bacteria Pantoea dispersa and Enterobacter asburiae Promote Sugarcane Growth by Inducing Nitrogen Uptake and Defense-Related Gene Expression. Frontiers in Microbiology **11**, 1–20.
Soares FS, Rangel de Souza ALS, de Souza SA, de Souza Vespoli L, Pinto VB, Matiello L, da Silva FR, Menossi M, de Souza Filho GA. 2024. Fine-Tuning of Arabidopsis thaliana Response to Endophytic Colonization by Gluconacetobacter diazotrophicus PAL5 Revealed by Transcriptomic Analysis. Plants **13**, 1–19.
Souza ALSR De, Souza SA De, Oliveira MVV De, Ferraz TM. 2016. Endophytic colonization of Arabidopsis thaliana by Gluconacetobacter diazotrophicus and its effect on plant growth promotion, plant physiology , and activation of plant defense. Plant Soil **399**, 257–270.
Srivastava S, Ranjan M, Bano N, Asif MH, Srivastava S. 2023. Comparative transcriptome analysis reveals the phosphate starvation alleviation mechanism of phosphate accumulating Pseudomonas putida in Arabidopsis thaliana. Scientific Reports **13**, 1–15.
Stringlis IA, Proietti S, Hickman R, Van Verk MC, Zamioudis C, Pieterse CMJ. 2018. Root transcriptional dynamics induced by beneficial rhizobacteria and microbial immune elicitors reveal signatures of adaptation to mutualists. Plant Journal **93**, 166–180.
Tang J, Wu D, Li X, *et al.* 2022. Plant immunity suppression via PHR1-RALF-FERONIA shapes the root microbiome to alleviate phosphate starvation. The EMBO Journal **41**, 1–19.
Thiebaut F, Rojas CA, Grativol C, *et al.* 2017. Roles of non-coding RNA in sugarcane-microbe interaction. Non-coding RNA **3**, 1–24.
Thiebaut F, Urquiaga MC de O, Rosman AC, da Silva ML, Hemerly AS. 2022. The Impact of Non-Nodulating Diazotrophic Bacteria in Agriculture: Understanding the Molecular Mechanisms That Benefit Crops. International Journal of Molecular Sciences **23**, 1–22.

Thomsen HC, Eriksson D, Møller IS, Schjoerring JK. 2014. Cytosolic glutamine synthetase: A target for improvement of crop nitrogen use efficiency? Trends in Plant Science **19**, 656–663.
Tian W, Li L, Xiao X, *et al.* 2022. Identification of a plant endophytic growth-promoting bacteria capable of inhibiting cadmium uptake in rice. Journal of Applied Microbiology **132**, 520–531.
Tilman D, Balzer C, Hill J, Befort BL. 2011. Global food demand and the sustainable intensification of agriculture. Proceedings of the National Academy of Sciences of the United States of America **108**, 20260–20264.
Tobin AK, Yamaya T. 2001. Cellular compartmentation of ammonium assimilation in rice and barley. Journal of Experimental Botany **52**, 591–604.
Tufail MA, Touceda-González M, Pertot I, Ehlers RU. 2021. Gluconacetobacter diazotrophicus pal5 enhances plant robustness status under the combination of moderate drought and low nitrogen stress in zea mays l. Microorganisms **9**.
Upadhyay SK, Srivastava AK, Rajput VD, Chauhan PK, Bhojiya AA, Jain D, Chaubey G, Dwivedi P, Sharma B, Minkina T. 2022. Root Exudates: Mechanistic Insight of Plant Growth Promoting Rhizobacteria for Sustainable Crop Production. Frontiers in Microbiology **13**.
Urquiaga S, Boddey R. 1992. Contribution of Nitrogen Fixation to Sugar Cane: Nitrogen15 and NitrogenBalance Estimates. doi: 10.2136/sssaj1992.03615995005600010017x.
Urquiaga S, Xavier RP, de Morais RF, *et al.* 2012. Evidence from field nitrogen balance and 15N natural abundance data for the contribution of biological N 2 fixation to Brazilian sugarcane varieties. Plant and Soil **356**, 5–21.
Vacheron J, Desbrosses G, Bouffaud ML, Touraine B, Moënne-Loccoz Y, Muller D, Legendre L, Wisniewski-Dyé F, Prigent-Combaret C. 2013. Plant growth-promoting rhizobacteria and root system functioning. Frontiers in Plant Science **4**, 1–19.
Vandenkoornhuyse P, Quaiser A, Duhamel M, Le Van A, Dufresne A. 2015. The importance of the microbiome of the plant holobiont. New Phytologist **206**, 1196–1206.
Vargas L, Brígida A, Mota J, *et al.* 2014. Drought tolerance conferred to sugarcane by association with Gluconacetobacter diazotrophicus: A transcriptomic view of hormone pathways. PLoS ONE, 1–37.
Vargas L, de Carvalho TLG, Ferreira PCG, Baldani VLD, Baldani JI, Hemerly AS. 2012. Early responses of rice (Oryza sativa L.) seedlings to inoculation with beneficial diazotrophic bacteria are dependent on plant and bacterial genotypes. Plant and Soil **356**, 127–137.
Voges MJEEE, Bai Y, Schulze-Lefert P, Sattely ES. 2019. Plant-derived coumarins shape the composition of an Arabidopsis synthetic root microbiome. Proceedings of the National Academy of Sciences of the United States of America **116**, 12558–12565.
Wilkinson JQ, Crawford NM. 1993. Identification and characterization of a chlorate-resistant mutant of Arabidopsis thaliana with mutations in both nitrate reductase structural genes NIA1 and NIA2. Molecular Genetics and Genomics **239**, 289–297.
Zhang J, Liu W, Bu J, Lin Y, Bai Y. 2023. Host genetics regulate the plant microbiome. Current Opinion in Microbiology **72**.

Zhang J, Liu YX, Zhang N, *et al.* 2019. NRT1.1B is associated with root microbiota composition and nitrogen use in field-grown rice. Nature Biotechnology **37**, 676–684.
Zhao H, Xu J, Huang L, Ding Y, Lin X, Sun C. 2025. Auxin and Root Hair Defective Six-Like 4 Regulate Azospirillum brasilense-Induced Root Hair Development in Arabidopsis. Plant, Cell and Environment, 1–2.
Zluhan-Martínez E, López-Ruíz BA, García-Gómez ML, García-Ponce B, de la Paz Sánchez M, Álvarez-Buylla ER, Garay-Arroyo A. 2021. Integrative Roles of Phytohormones on Cell Proliferation, Elongation and Differentiation in the Arabidopsis thaliana Primary Root. Frontiers in Plant Science **12**, 1–20.
Zuluaga MYA, Milani KML, Gonçalves LSA, De Oliveira ALM. 2020. Diversity and plant growth-promoting functions of diazotrophic/N-scavenging bacteria isolated from the soils and rhizospheres of two species of Solanum. PLoS ONE **15**, 1–25.

6. Figure legends

Fig 1. Conserved modulation of *AIP10* expression by plant growth–promoting bacteria and its nuclear protein structure in *A. thaliana* and sugarcane. (A) Expression profile of the *AIP10* homolog in sugarcane root and shoot tissues of two BNF contrasting genotypes (SP70-1143, high BNF; Chunee, low BNF) from plants naturally colonized by PGPB (Stalk) and plants grown under bacteria-free conditions (BF). Expression values are shown as $\log_2$ fold change. **(B)** Predicted protein structures of *AIP10* putative homologs encoded by two isoforms *AT1G80940.1* and *AT1G80940.3* from *A. thaliana*, and by *Sspoon.04G0001710-3D* from *Saccharum spontaneum*. Protein domains were predicted using the SMART program. The scheme shows the nuclear localization signal (NLS), coiled-coil, and ribosomal L32e domains, suggesting a possible role related to nuclear regulation and protein interaction, potentially conserved between species. **(C)** Expression levels of *AIP10* in *A. thaliana Col-0* plants at 7 DAI after inoculation with two different PGPB strains, *G. diazotrophicus* and *H. seropedicae*.

Fig 2. Taxonomic distribution and enrichment patterns of key microbial functional groups in roots and bulk soil of non-inoculated Col-0 and *aip10-1* plants. (A) Venn diagram shows shared and unique microbial species associated with roots and surrounding soil from Col-0 and *aip10-1* plants. **(B–D)** Relative abundance (left panels) and z-score heatmaps (right panels) for bacterial groups with functional relevance to plant performance, including **(B)** potential diazotrophic bacterial species, **(C)** potential plant growth-promoting bacteria (PGPB), and **(D)** potential pathogenic bacterial species. Data are shown for root and soil compartments of Col-0 wild type and *aip10-1* plants. In the heat map, red represents higher abundance, and blue represents lower abundance, according to the z-score value.

Fig 3. Functional analyses of *AIP10* silencing in *A. thaliana* root colonization and association with diazotrophic PGPB strains *H. seropedicae* HRC54 and *G. diazotrophicus* Pal5. (A) Representative images of Col-0 and *aip10-1* plants mock-treated, inoculated with *H. seropedicae* HRC54 or *G. diazotrophicus* Pal5 at 20 days after germination (DAG). Scale bars: 1cm. *Note that images in the three panels have different Bars.* **(B–E)** Growth and developmental parameters of Col-0 and *aip10-1* plants inoculated with *H. seropedicae* HRC54 or *G. diazotrophicus* Pal5. **(B)** Primary root length and **(C)** lateral root number measured at 15

DAG, the box plot graphs show the distribution of data of 10 individuals. **(D)** Dry weight of the shoots, using nine biological replicates, and **(E)** rosette area, using five biological replicates, measured at 21 DAG. Data are presented as box plots showing median, interquartile range, and minimum/maximum values. **(F, G)** Absolute qPCR quantification of *H. seropedicae* HRC54 and *G. diazotrophicus* Pal5 colonization in roots of Col-0 and *aip10-1* at 7 DAI, respectively. The data represents the number of bacterial cells per gram of root tissue, obtained by absolute qPCR quantification. Bars represent mean ± standard deviation of three biological replicates and each biological replicate (pool of five plants) was analyzed with three technical replicates. **(H, I)** Relative expression of the *nifH* gene in *H. seropedicae* HRC54 and *G. diazotrophicus* Pal5 colonizing Col-0 and *aip10-1* roots at 7 DAI, quantified by RT-qPCR. Gene expression values are shown as fold-change relative to GAPDH and UBI14 reference genes. Bars represent mean ± standard deviation of the relative mRNA expression in three biological replicates and each biological replicate (pool of five plants) was analyzed with three technical replicates. **(J)** Representative confocal microscopy images showing *G. diazotrophicus* (RFP-labeled) and *H. seropedicae* (GFP-labeled) colonization patterns in Col-0 and *aip10-1* roots at 11 DAG and 7 DAI. Images include RFP, GFP, DIC, and merged channels. Scale bars: 50 µm. The box plot graphs represent the interquartile range (IQR), with the inner line running down the median. The whiskers extend to the maximum and minimum values, including all points within that range. The differences between groups in all analyses were confirmed by One-Way ANOVA ($p < 0.05$), and different letters indicate statistically different means according to Tukey's test at 5% probability. DAG, Days After Germination. Statistical analyses were performed using Student's t-test at a 5% significance level. (*) indicates statistically significant differences ($p \leq 0.05$).

Fig 4. RT-qPCR analysis of genes involved in cell division (ABAP1 regulatory network), cell wall organization, bacterial response, and root morphogenesis in *aip10-1* and wild-type Col-0 roots, at 7 DAI. (A) *ABAP1*; **(B)** *CDT1a*; **(C)** *CYCB1;1*; **(D)** *LRX4*; **(E)** *ILA* and **(F)** *RSL4*. RT-qPCR results are presented as the ratio of expression of each gene relative to the constitutive expression of *GAPDH* and *UBI14* reference genes when compared to mock and inoculated plants. Bars represent mean ± standard deviation of the relative mRNA expression in three biological replicates and each biological replicate analyzed with three technical replicates. Statistical analysis was performed using the Student's t-test ($P \leq 0.05$). Means with different letters are significantly different at 5% level of confidence.

Fig 5. Shoot development of *aip10-1* and wild-type Col-0 plants inoculated with different plant growth-promotion bacteria, grown in a greenhouse under low and high fertilization conditions (0.06 g/L and 0.12 g/L NPK, respectively). (A) Representative images of *A. thaliana* Col-0 and *aip10-1* plants inoculated with *H. seropedicae* HRC54 at 35 DAG (31 DAI), grown in a greenhouse under two different fertilization conditions. **(B)** Representative images of *A. thaliana* Col-0 and *aip10-1* plants inoculated with *G. diazotrophicus* Pal5 at 35 DAG (31 DAI), grown in a greenhouse under two different fertilization conditions. **(C to E)** mock and HRC54-inoculated plants at 35 DAG. **(C)** Rosette area measurement using ImageJ program; **(D)** Shoot dry weight; **(E)** Total chlorophyll content in leaf disks. **(F to H)** mock and Pal5-inoculated plants at 35 DAG. **(F)** Rosette area measurement using ImageJ program; **(G)** Shoot dry weight; **(H)** Total chlorophyll content in leaf disks. The box plot graphs show the distribution of data of six individuals. The box represents the interquartile range (IQR), with the inner line running down the median. The whiskers extend to the maximum and minimum values, including all points within that range. Differences between groups were confirmed by

Student's t-test and means followed by different letters indicate significant differences at the 5% confidence level.

Fig 6. Root development of Col-0 and *aip10-1* plants inoculated with different plant growth-promoting bacteria, grown in a greenhouse under low and high fertilization conditions at 35 DAG. (A) Root dry weight in mock and HRC54-inoculated plants. **(B)** Root length in mock and HRC54-inoculated plants. **(C)** Root surface area in mock and HRC54-inoculated plants. **(D)** Root dry weight in mock and Pal5-inoculated plants. **(E)** Root length in mock and Pal5-inoculated plants. **(F)** Root surface area in mock and Pal5-inoculated plants. Root length and surface area were measured by WinRHIZO. The box plot graphs show the distribution of data of five individuals. The box represents the interquartile range (IQR), with the inner line running down the median. The whiskers extend to the maximum and minimum values, including all points within that range. Differences between groups were confirmed by Student's t-test and means followed by different letters indicate significant differences at the 5% confidence level.

Fig 7. Reproductive stage of Col-0 and *aip10-1* plants inoculated with different plant growth-promoting bacteria, cultivated in a greenhouse under low and high fertilization conditions at 60 DAG. (A) Representative images of Col-0 and *aip10-1* during the reproductive stage comparing the different responses to HRC54 and Pal5 inoculation, in response to low and high fertilization treatments. **(B to D)** mock and HRC54-inoculated plants; **(B)** Length of the main inflorescence axis; **(C)** Total number of siliques in the main inflorescence axis; **(D)** Total seed weight per individual. **(E to G)** mock and Pal5-inoculated plants; **(E)** Length of the main inflorescence axis; **(F)** Total number of siliques in the main inflorescence axis; **(G)** Total seed weight per individual. The box plot graphs show the distribution of data of five individuals. The box represents the interquartile range (IQR), with the inner line running down the median. The whiskers extend to the maximum and minimum values, including all points within that range. Differences between groups were confirmed by Student's t-test and means followed by different letters indicate significant differences at the 5% confidence level.

Figure 8. Expression of nitrogen metabolism-related genes in mock-treated Col-0 and *aip10-1* roots, cultivated in greenhouse under high and low fertilization conditions at 20 DAG. qRT-PCR analyses were performed in mock-treated Col-0 and *aip10-1* roots, cultivated under high and low fertilization conditions at 20 DAG. (**A**) *nifH* transcript abundance. **(B)** *NIA1* transcript levels. **(C)** *NIA2* transcript levels. (**D**) *GLN1;1* transcript levels. (**E**) *GLN1;3* transcript levels. Relative expression values were quantified by RT-qPCR and normalized by *UBI14* and *GAPDH* reference genes. Bars represent mean ± standard deviation of the relative mRNA expression in three biological replicates and each biological replicate analyzed with three technical replicates. Statistical analysis was performed using the Student's t-test ($P \leq 0.05$). Means with different letters are significantly different at 5% level of confidence. This mock-treated Col-0 and *aip10-1* expression data is the same as the one presented in Fig.9.

Fig. 9. Expression of nitrogen metabolism-related genes in Col-0 and *aip10-1* roots of inoculated plants, cultivated in greenhouse under high and low fertilization conditions at 20 DAG. (A, B) *nifH* transcript abundance from *H. seropedicae* HRC54 and *G. diazotrophicus* Pal5, respectively, colonizing Col-0 and *aip10-1* roots. **(C,D)** *GLN1;1* mRNA level in *H. seropedicae* HRC54 and *G. diazotrophicu*s Pal5 inoculated roots, respectively. **(E, F)** *NIA1*

transcript levels in *H. seropedicae* HRC54 and *G. diazotrophicu*s Pal5 inoculated roots, respectively. Relative expression values were quantified by RT-qPCR and normalized by UBI14 and GAPDH reference genes. Bars represent mean ± standard deviation of the relative mRNA expression in three biological replicates and each biological replicate analyzed with three technical replicates. Statistical analysis was performed using the Student's t-test. Means with different letters are significantly different at 5% level of confidence. This mock-treated Col-0 and *aip10-1* expression data is the same as the one presented in Fig.8.

Fig 10. A hypothetical model illustrating the potential mechanisms that coordinate plant growth and metabolism with the recruitment of beneficial root microbiota in the *AIP10* knockout mutant of *A. thaliana,* under low nutrient conditions. AIP10 is proposed to function as a regulatory node connecting cell cycle control and primary metabolism, likely through interactions with ABAP1, SnRK1 (via KIN10), and possibly additional partners. Elimination of AIP10 in *aip10-1* mutant triggers broad transcriptional changes across multiple pathways. Attenuation of AIP10/ABAP1 signaling enhances pre-replication complex (Pre-RC) assembly by relieving repression of pre-RC genes (*CDT1a)*, resulting in increased DNA replication and higher cell division rates (*CYCB1;1*). This process is accompanied by transcriptional reprogramming of metabolic pathways leading to greater carbohydrate accumulation, along with modulation of immune and defense responses, and nitrogen assimilation genes (*NIA1* and *GLN1;1*), in a manner that favors the association with beneficial plant growth promoting bacteria. At the root level, non-inoculated *aip10-1* plants exhibit enrichment of beneficial microbial taxa, including diazotrophic bacteria, and a reduced abundance of pathogenic taxa, comparing to Col-0. Under low nitrogen conditions, PGPB inoculation further enhances bacterial colonization and further induces *nifH* expression in *aip10-1* compared to Col-0. The molecular and microbiome shifts promote improved root system architecture, increased shoot biomass and chlorophyll content, and enhanced reproductive performance, with the strongest growth responses observed in inoculated *aip10-1* plants under low nitrogen availability. Orange arrows indicate responses in mock-treated *aip10-1* plants compared to Col-0, whereas blue arrows represent responses in inoculated *aip10-1* plants compared to Col-0 plants. Arrow thickness corresponds to the magnitude of the response. Created with BioRender.com.

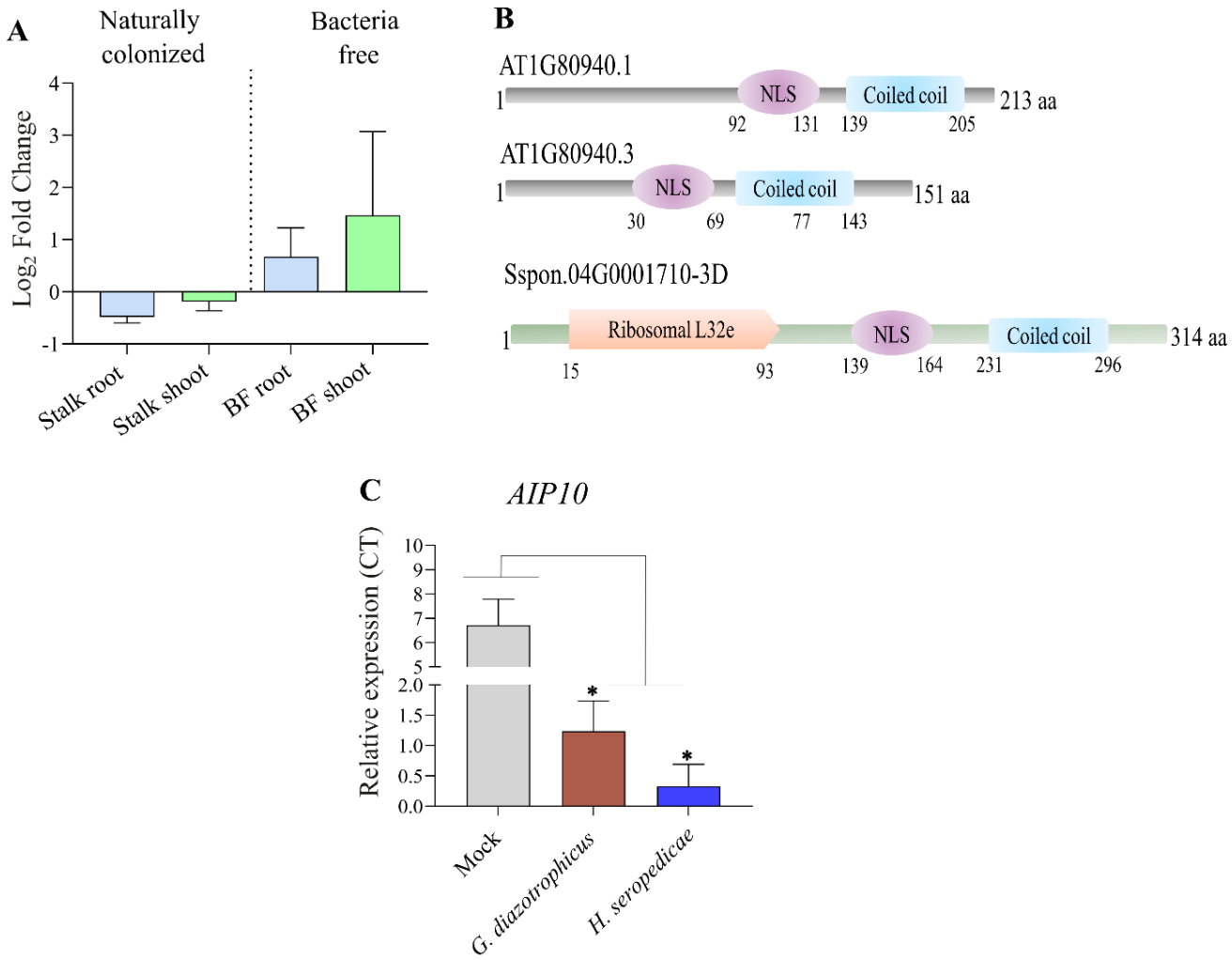

Figure 1. Conserved modulation of *AIP10* expression by plant growth–promoting bacteria and its nuclear protein structure in *A. thaliana* and sugarcane. (A) Expression profile of the *AIP10* homolog in sugarcane root and shoot tissues of two BNF contrasting genotypes (SP70-1143, high BNF; Chunee, low BNF) from plants naturally colonized by PGPB (Stalk) and plants grown under bacteria-free conditions (BF). Expression values are shown as $\log_2$ fold change. **(B)** Predicted protein structures of *AIP10* putative homologs encoded by two isoforms *AT1G80940.1* and *AT1G80940.3* from *A. thaliana*, and by *Sspoon.04G0001710-3D* from *Saccharum spontaneum*. Protein domains were predicted using the SMART program. The scheme shows the nuclear localization signal (NLS), coiled-coil, and ribosomal L32e domains, suggesting a possible role related to nuclear regulation and protein interaction, potentially conserved between species. **(C)** Expression levels of *AIP10* in *A. thaliana Col-0* plants at 7 DAI after inoculation with two different PGPB strains, *G. diazotrophicus* and *H. seropedicae*.

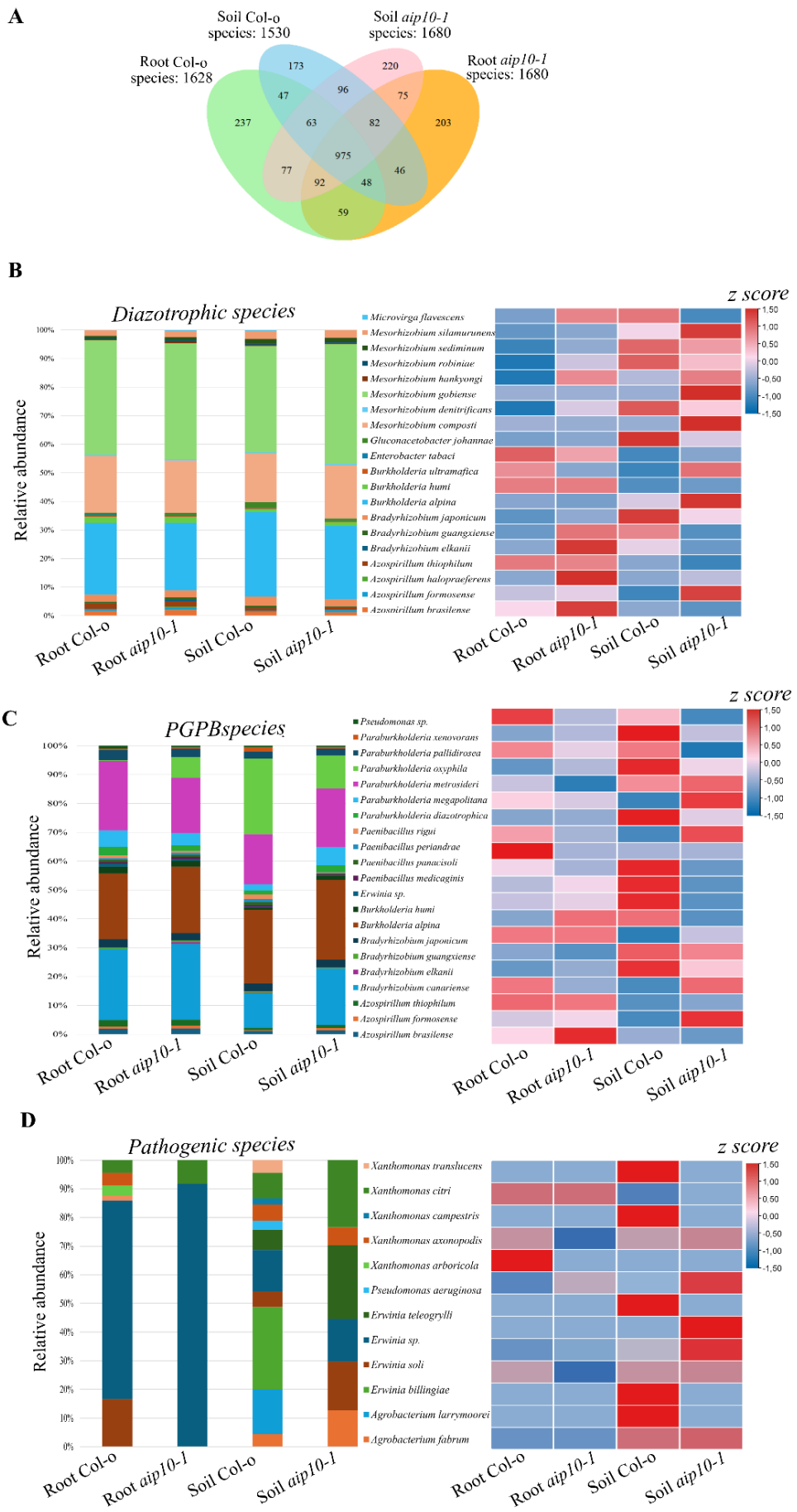
A
Soil Col-o
species: 1530
Soil aip10-1
species: 1680
Root Col-o
species: 1628
Root aip10-1
species: 1680
173
220
47
96
75
237
63
82
203
975
77
46
92
48
59
B
Diazotrophic species
z score
Relative abundance
Microvirga flavescens
Mesorhizobium silamurunens
Mesorhizobium sediminum
Mesorhizobium robiniae
Mesorhizobium hankyongi
Mesorhizobium gobiense
Mesorhizobium denitrificans
Mesorhizobium composti
Gluconacetobacter johannae
Enterobacter tabaci
Burkholderia ultramafica
Burkholderia humi
Burkholderia alpina
Bradyrhizobium japonicum
Bradyrhizobium guangxiense
Bradyrhizobium elkanii
Azospirillum thiophilum
Azospirillum halopraeferens
Azospirillum formosense
Azospirillum brasilense
Root Col-o
Root aip10-1
Soil Col-o
Soil aip10-1
C
PGPBspecies
z score
Relative abundance
Pseudomonas sp.
Paraburkholderia xenovorans
Paraburkholderia pallidirosea
Paraburkholderia oxyphila
Paraburkholderia metrosideri
Paraburkholderia megapolitana
Paraburkholderia diazotrophica
Paenibacillus rigui
Paenibacillus periandrae
Paenibacillus panacisoli
Paenibacillus medicaginis
Erwinia sp.
Burkholderia humi
Burkholderia alpina
Bradyrhizobium japonicum
Bradyrhizobium guangxiense
Bradyrhizobium elkanii
Bradyrhizobium canariense
Azospirillum thiophilum
Azospirillum formosense
Azospirillum brasilense
Root Col-o
Root aip10-1
Soil Col-o
Soil aip10-1
D
Pathogenic species
z score
Relative abundance
Xanthomonas translucens
Xanthomonas citri
Xanthomonas campestris
Xanthomonas axonopodis
Xanthomonas arboricola
Pseudomonas aeruginosa
Erwinia teleogrylli
Erwinia sp.
Erwinia soli
Erwinia billingiae
Agrobacterium larrymoorei
Agrobacterium fabrum
Root Col-o
Root aip10-1
Soil Col-o
Soil aip10-1

Figure 2. Taxonomic distribution and enrichment patterns of key microbial functional groups in roots and bulk soil of non-inoculated Col-0 and *aip10-1* plants. (A) Venn diagram shows shared and unique microbial species associated with roots and surrounding soil from Col-0 and *aip10-1* plants. **(B–D)** Relative abundance (left panels) and z-score heatmaps (right panels) for bacterial groups with functional relevance to plant performance, including **(B)** potential diazotrophic bacterial species, **(C)** potential plant growth-promoting bacteria (PGPB), and **(D)** potential pathogenic bacterial species. Data are shown for root and soil compartments of Col-0 wild type and *aip10-1* plants. In the heat map, red represents higher abundance, and blue represents lower abundance, according to the z-score value.

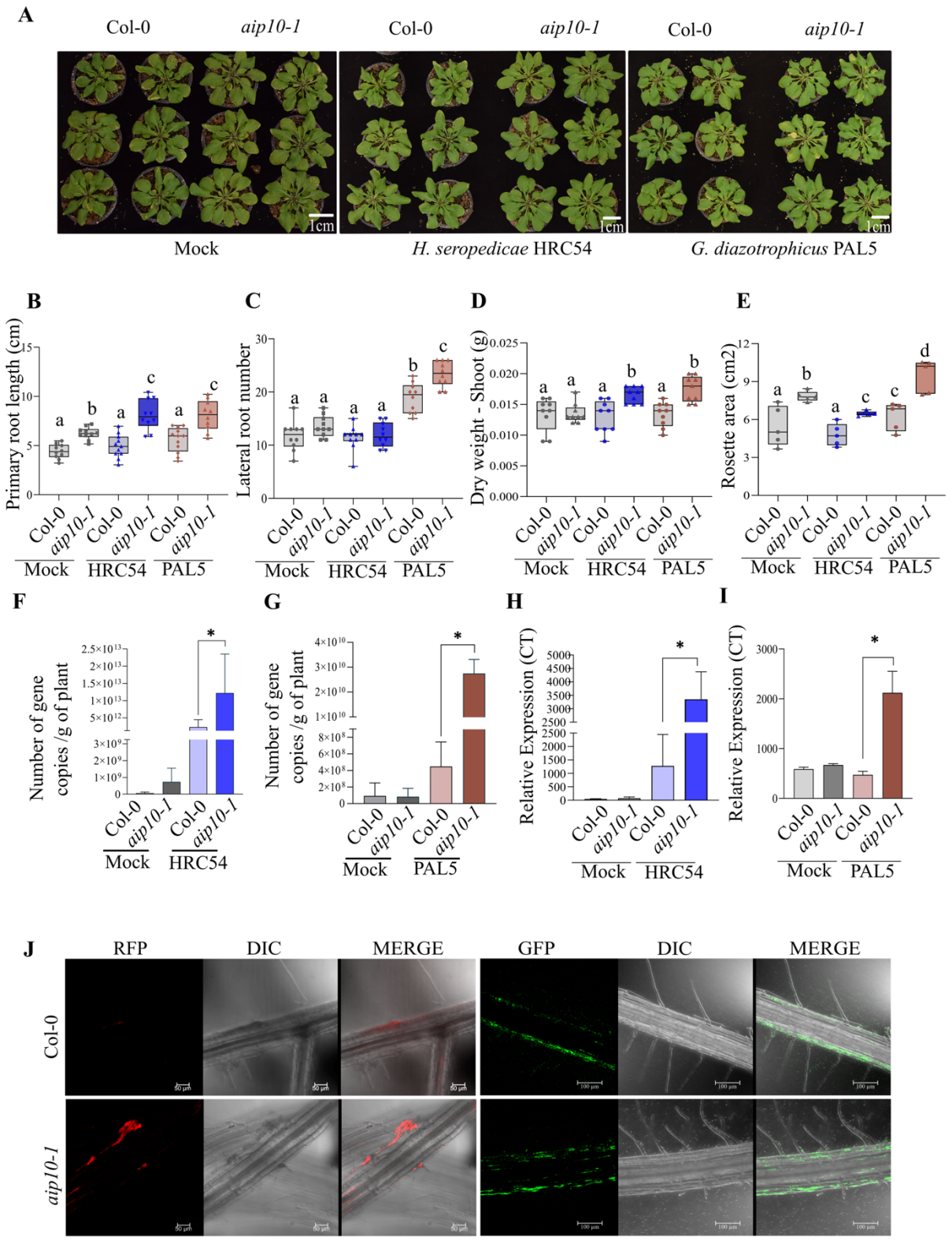

Figure 3. Functional analyses of *AIP10* silencing in *A. thaliana* root colonization and association with diazotrophic PGPB strains *H. seropedicae* HRC54 and *G. diazotrophicus* Pal5. (A) Representative images of Col-0 and *aip10-1* plants mock-treated, inoculated with *H. seropedicae* HRC54 or *G. diazotrophicus* Pal5 at 20 days after germination (DAG). Scale bars: 1cm. *Note that images in the three panels have different Bars.* **(B–E)** Growth and developmental parameters of Col-0 and *aip10-1* plants inoculated with *H. seropedicae* HRC54

or *G. diazotrophicus* Pal5. **(B)** Primary root length and **(C)** lateral root number measured at 15 DAG, the box plot graphs show the distribution of data of 10 individuals. **(D)** Dry weight of the shoots, using nine biological replicates, and **(E)** rosette area, using five biological replicates, measured at 21 DAG. Data are presented as box plots showing median, interquartile range, and minimum/maximum values. **(F, G)** Absolute qPCR quantification of *H. seropedicae* HRC54 and *G. diazotrophicus* Pal5 colonization in roots of Col-0 and *aip10-1* at 7 DAI, respectively. The data represents the number of bacterial cells per gram of root tissue, obtained by absolute qPCR quantification. Bars represent mean ± standard deviation of three biological replicates and each biological replicate (pool of five plants) was analyzed with three technical replicates. **(H, I)** Relative expression of the *nifH* gene in *H. seropedicae* HRC54 and *G. diazotrophicus* Pal5 colonizing Col-0 and *aip10-1* roots at 7 DAI, quantified by RT-qPCR. Gene expression values are shown as fold-change relative to GAPDH and UBI14 reference genes. Bars represent mean ± standard deviation of the relative mRNA expression in three biological replicates and each biological replicate (pool of five plants) was analyzed with three technical replicates. **(J)** Representative confocal microscopy images showing *G. diazotrophicus* (RFP-labeled) and *H. seropedicae* (GFP-labeled) colonization patterns in Col-0 and *aip10-1* roots at 11 DAG and 7 DAI. Images include RFP, GFP, DIC, and merged channels. Scale bars: 50 µm. The box plot graphs represent the interquartile range (IQR), with the inner line running down the median. The whiskers extend to the maximum and minimum values, including all points within that range. The differences between groups in all analyses were confirmed by One-Way ANOVA ($p < 0.05$), and different letters indicate statistically different means according to Tukey's test at 5% probability. DAG, Days After Germination. Statistical analyses were performed using Student's t-test at a 5% significance level. (*) indicates statistically significant differences ($p \leq 0.05$).

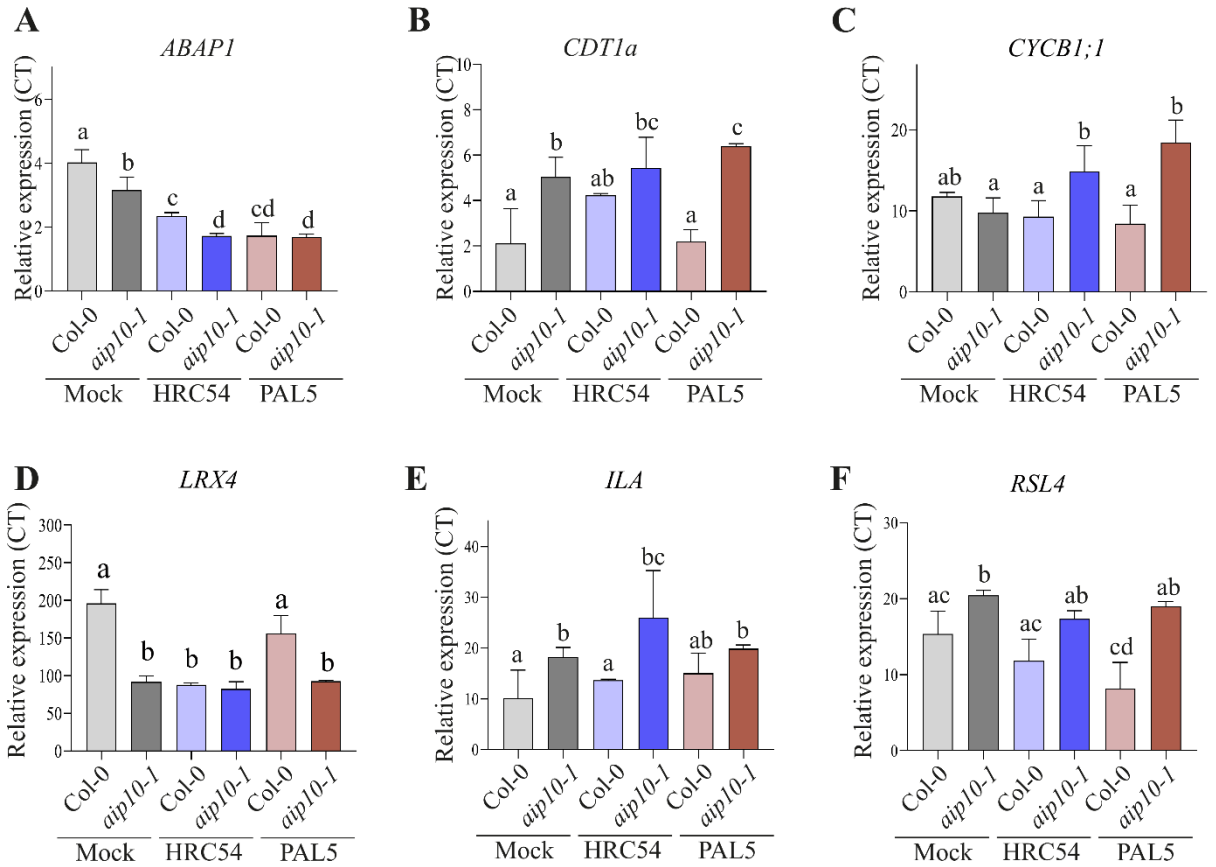

Figure 4. RT-qPCR analysis of genes involved in cell division (ABAP1 regulatory network), cell wall organization, bacterial response, and root morphogenesis in *aip10-1* and wild-type Col-0 roots, at 7 DAI. (A) *ABAP1*; **(B)** *CDT1a*; **(C)** *CYCB1;1*; **(D)** *LRX4*; **(E)** *ILA* and **(F)** *RSL4*. RT-qPCR results are presented as the ratio of expression of each gene relative to the constitutive expression of *GAPDH* and *UBI14* reference genes when compared to mock and inoculated plants. Bars represent mean ± standard deviation of the relative mRNA expression in three biological replicates and each biological replicate analyzed with three technical replicates. Statistical analysis was performed using the Student's t-test ($P \leq 0.05$). Means with different letters are significantly different at 5% level of confidence.

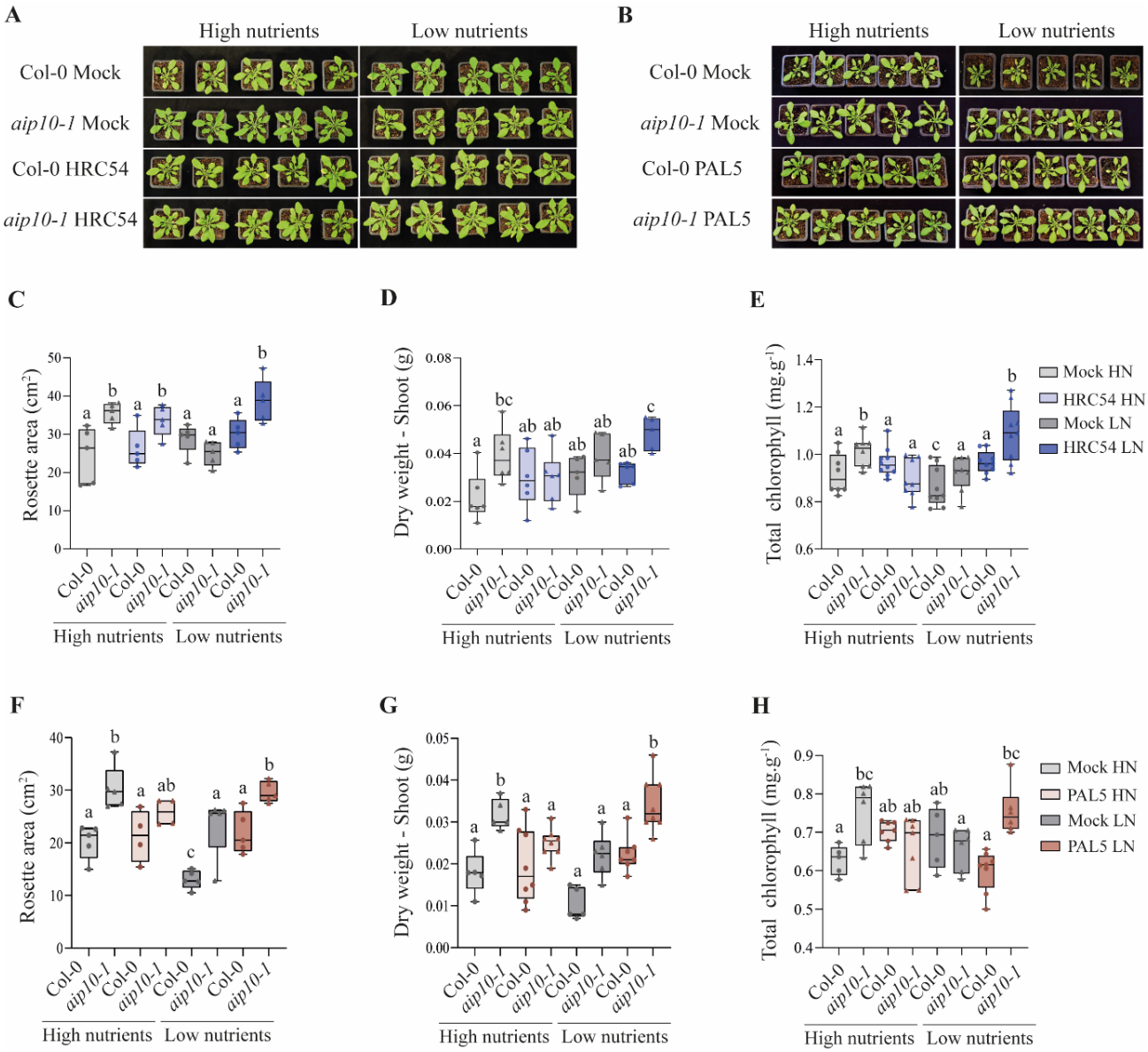

Figure 5. Shoot development of *aip10-1* and wild-type Col-0 plants inoculated with different plant growth-promotion bacteria, grown in a greenhouse under low and high fertilization conditions (0.06 g/L and 0.12 g/L NPK, respectively). (A) Representative images of *A. thaliana* Col-0 and *aip10-1* plants inoculated with *H. seropedicae* HRC54 at 35 DAG (31 DAI), grown in a greenhouse under two different fertilization conditions. **(B)** Representative images of *A. thaliana* Col-0 and *aip10-1* plants inoculated with *G. diazotrophicus* Pal5 at 35 DAG (31 DAI), grown in a greenhouse under two different fertilization conditions. **(C to E)** mock and HRC54-inoculated plants at 35 DAG. **(C)** Rosette area measurement using ImageJ program; **(D)** Shoot dry weight; **(E)** Total chlorophyll content in leaf disks. **(F to H)** mock and Pal5-inoculated plants at 35 DAG. **(F)** Rosette area measurement using ImageJ program; **(G)** Shoot dry weight; **(H)** Total chlorophyll content in leaf disks. The box plot graphs show the distribution of data of six individuals. The box represents the interquartile range (IQR), with the inner line running down the median. The whiskers extend to the maximum and minimum values, including all points within that range. Differences between groups were confirmed by Student's t-test and means followed by different letters indicate significant differences at the 5% confidence level

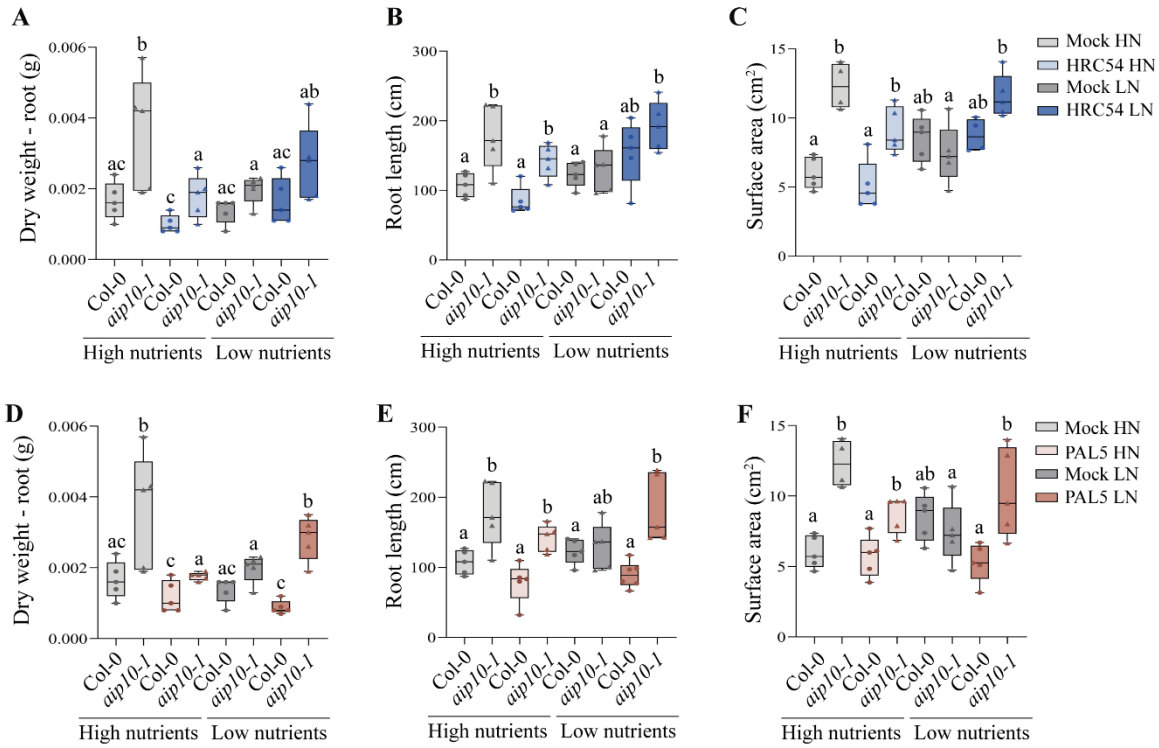

Figure 6. Root development of Col-0 and *aip10-1* plants inoculated with different plant growth-promoting bacteria, grown in a greenhouse under low and high fertilization conditions at 35 DAG. (A) Root dry weight in mock and HRC54-inoculated plants. **(B)** Root length in mock and HRC54-inoculated plants. **(C)** Root surface area in mock and HRC54-inoculated plants. **(D)** Root dry weight in mock and Pal5-inoculated plants. **(E)** Root length in mock and Pal5-inoculated plants. **(F)** Root surface area in mock and Pal5-inoculated plants. Root length and surface area were measured by WinRHIZO. The box plot graphs show the distribution of data of five individuals. The box represents the interquartile range (IQR), with the inner line running down the median. The whiskers extend to the maximum and minimum values, including all points within that range. Differences between groups were confirmed by Student's t-test and means followed by different letters indicate significant differences at the 5% confidence level.

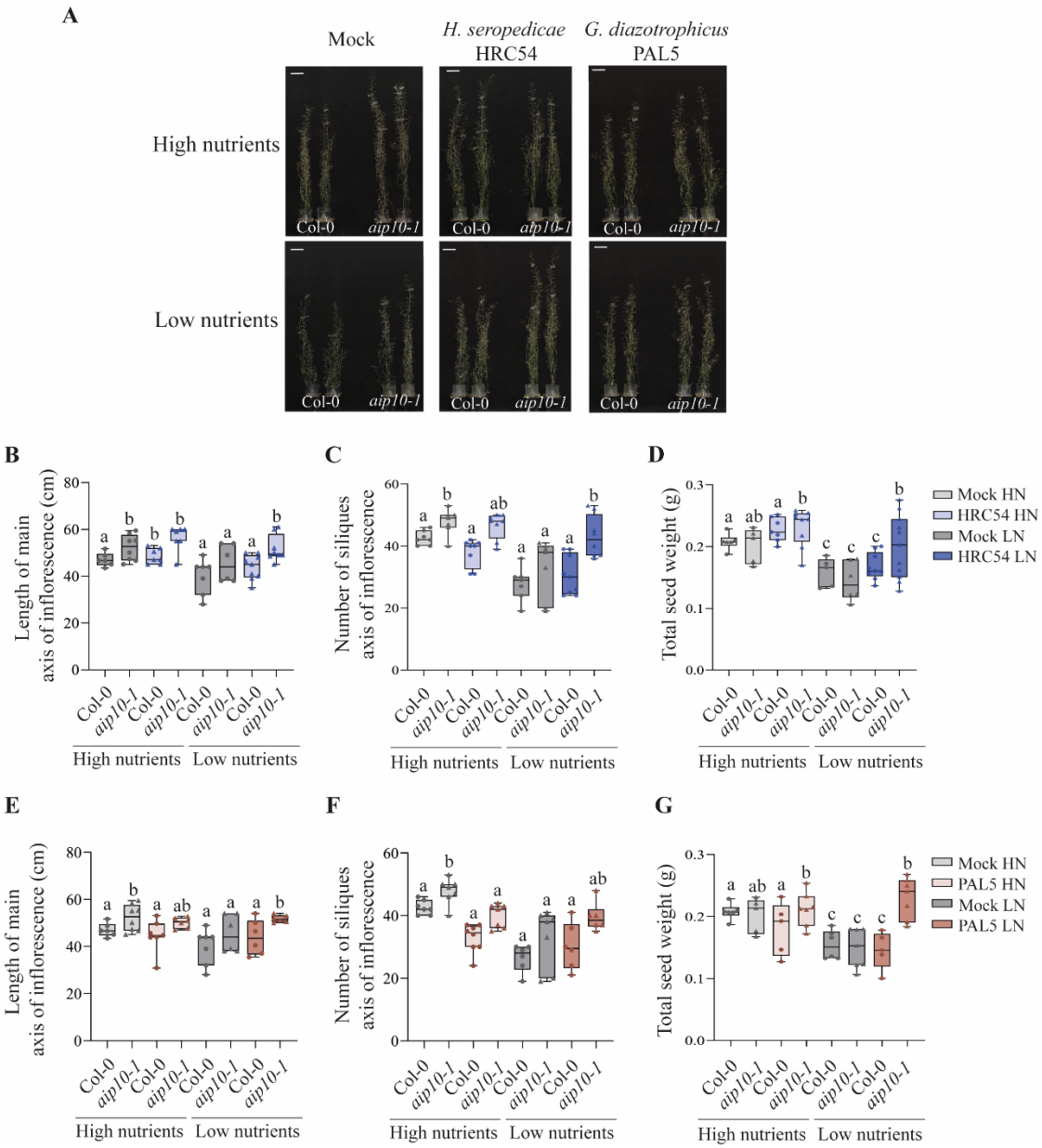

Figure 7. Reproductive stage of Col-0 and *aip10-1* plants inoculated with different plant growth-promoting bacteria, cultivated in a greenhouse under low and high fertilization conditions at 60 DAG. (A) Representative images of Col-0 and *aip10-1* during the reproductive stage comparing the different responses to HRC54 and Pal5 inoculation, in response to low and high fertilization treatments. **(B to D)** mock and HRC54-inoculated plants; **(B)** Length of the main inflorescence axis; **(C)** Total number of siliques in the main inflorescence axis; **(D)** Total seed weight per individual. **(E to G)** mock and Pal5-inoculated plants; **(E)** Length of the main inflorescence axis; **(F)** Total number of siliques in the main inflorescence axis; **(G)** Total seed weight per individual. The box plot graphs show the distribution of data of five individuals. The box represents the interquartile range (IQR), with the inner line running down the median. The whiskers extend to the maximum and minimum values, including all points within that range. Differences between groups were confirmed by Student's t-test and means followed by different letters indicate significant differences at the 5% confidence level.

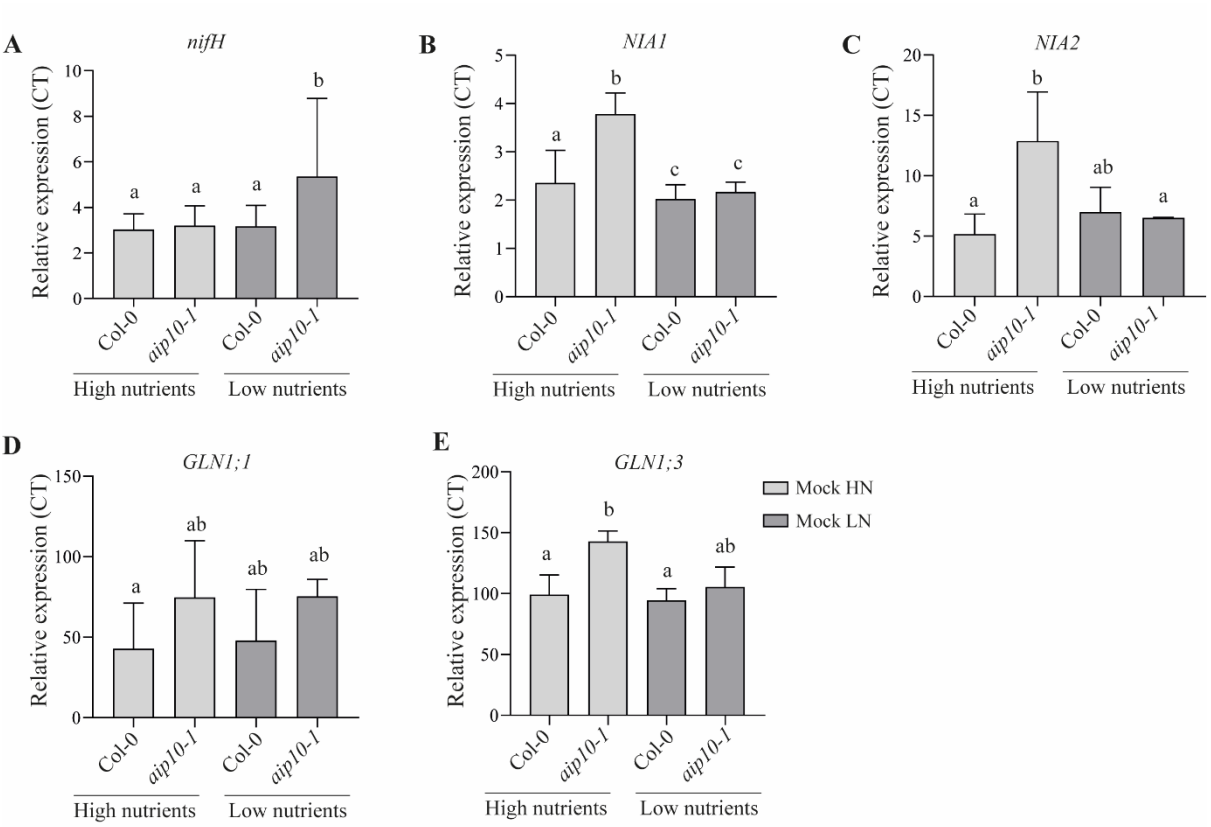

Figure 8. Expression of nitrogen metabolism-related genes in mock-treated Col-0 and *aip10-1* roots, cultivated in greenhouse under high and low fertilization conditions at 20 DAG. qRT-PCR analyses were performed in mock-treated Col-0 and *aip10-1* roots, cultivated under high and low fertilization conditions at 20 DAG. (**A**) *nifH* transcript abundance. **(B)** *NIA1* transcript levels. **(C)** *NIA2* transcript levels. (**D**) *GLN1;1* transcript levels. (**E**) *GLN1;3* transcript levels. Relative expression values were quantified by RT-qPCR and normalized by *UBI14* and *GAPDH* reference genes. Bars represent mean ± standard deviation of the relative mRNA expression in three biological replicates and each biological replicate analyzed with three technical replicates. Statistical analysis was performed using the Student's t-test ($P \leq 0.05$). Means with different letters are significantly different at 5% level of confidence. This mock-treated Col-0 and *aip10-1* expression data is the same as the one presented in Fig.9.

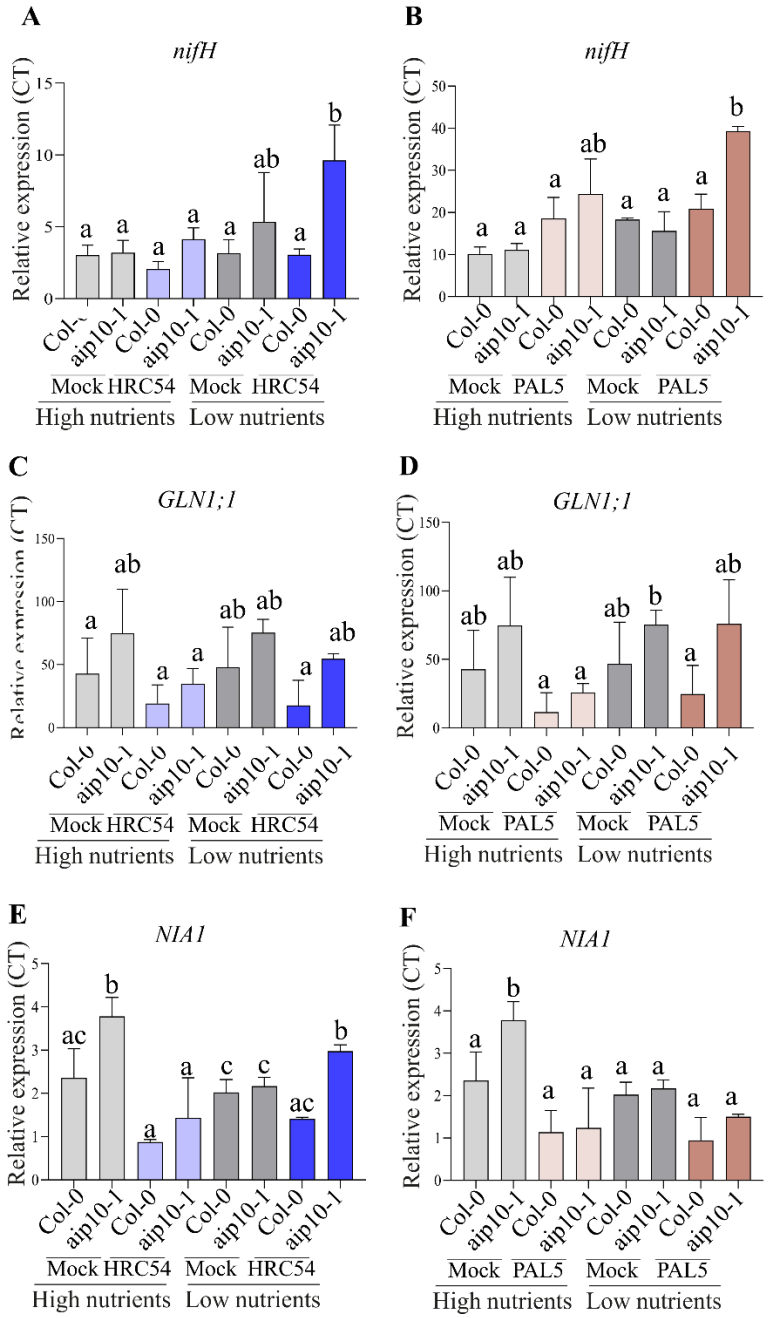

Figure 9. Expression of nitrogen metabolism-related genes in Col-0 and *aip10-1* roots of inoculated plants, cultivated in greenhouse under high and low fertilization conditions at 20 DAG. (A, B) *nifH* transcript abundance from *H. seropedicae* HRC54 and *G. diazotrophicus* Pal5, respectively, colonizing Col-0 and *aip10-1* roots. **(C, D)** *GLN1;1* mRNA level in *H. seropedicae* HRC54 and *G. diazotrophicus* Pal5 inoculated roots, respectively. **(E, F)** *NIA1* transcript levels in *H. seropedicae* HRC54 and *G. diazotrophicus* Pal5 inoculated roots, respectively. Relative expression values were quantified by RT-qPCR and normalized by UBI14 and GAPDH reference genes. Bars represent mean ± standard deviation of the relative mRNA expression in three biological replicates and each biological replicate analyzed with three technical replicates. Statistical analysis was performed using the Student's t-test. Means with different letters are significantly different at 5% level of confidence. This mock-treated Col-0 and *aip10-1* expression data is the same as the one presented in Fig.8.

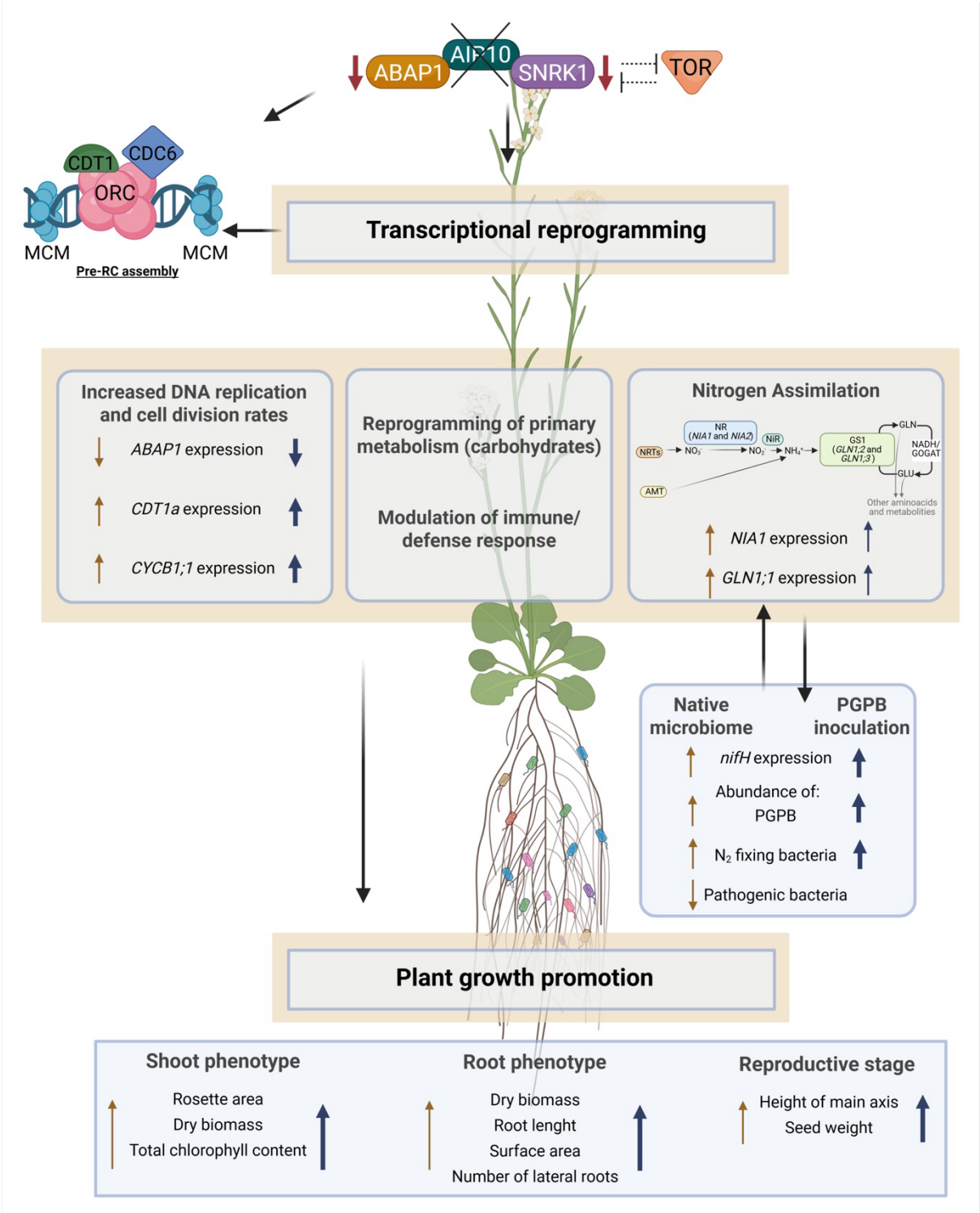

Figure 10. A hypothetical model illustrating the potential mechanisms that coordinate plant growth and metabolism with the recruitment of beneficial root microbiota in the *AIP10* knockout mutant of *A. thaliana,* under low nutrient conditions. AIP10 is proposed to function as a regulatory node connecting cell cycle control and primary metabolism, likely through interactions with ABAP1, SnRK1 (via KIN10), and possibly additional partners. Elimination of AIP10 in *aip10-1* mutant triggers broad transcriptional changes across multiple pathways. Attenuation of AIP10/ABAP1 signaling enhances pre-replication complex (Pre-RC) assembly by relieving repression of pre-RC genes (*CDT1a)*, resulting in increased DNA

replication and higher cell division rates (*CYCB1;1*). This process is accompanied by transcriptional reprogramming of metabolic pathways leading to greater carbohydrate accumulation, along with modulation of immune and defense responses, and nitrogen assimilation genes (*NIA1* and *GLN1;1*), in a manner that favors the association with beneficial plant growth promoting bacteria. At the root level, non-inoculated *aip10-1* plants exhibit enrichment of beneficial microbial taxa, including diazotrophic bacteria, and a reduced abundance of pathogenic taxa, comparing to Col-0. Under low nitrogen conditions, PGPB inoculation further enhances bacterial colonization and further induces *nifH* expression in *aip10-1* compared to Col-0. The molecular and microbiome shifts promote improved root system architecture, increased shoot biomass and chlorophyll content, and enhanced reproductive performance, with the strongest growth responses observed in inoculated *aip10-1* plants under low nitrogen availability. Orange arrows indicate responses in mock-treated *aip10-1* plants compared to Col-0, whereas blue arrows represent responses in inoculated *aip10-1* plants compared to Col-0 plants. Arrow thickness corresponds to the magnitude of the response. Created with BioRender.com.